Article

Current Biology

Dispersal of a dominant competitor can drive multispecies coexistence in biofilms

Highlights

- *P. aeruginosa*, *E. coli*, and *E. faecalis* can coexist in biofilms
- Modeling suggests that coexistence depends on biased dispersal of *P. aeruginosa*
- Ecological time course and invasion experiments support coexistence models
- Genetic manipulation experiments indicate a competition-dispersal trade-off

Authors

Jacob D. Holt, Daniel Schultz, Carey D. Nadell

Correspondence

carey.d.nadell@dartmouth.edu

In brief

Understanding the coexistence of many species despite competition for space and limiting nutrients in bacterial biofilms is an enduring challenge. Holt et al. show that a dominant competitor can permit coexistence in long-lived biofilm communities, including with species it would otherwise displace, if it undergoes repeated biased dispersal.

Holt et al., 2024, Current Biology *34*, 1–14
September 23, 2024
https://doi.org/10.1016/j.cub.2024.07.078

CellPress

Please cite this article in press as: Holt et al., Dispersal of a dominant competitor can drive multispecies coexistence in biofilms, Current Biology (2024), https://doi.org/10.1016/j.cub.2024.07.078

Current Biology

CellPress

Article

Dispersal of a dominant competitor can drive multispecies coexistence in biofilms

Jacob D. Holt,[1,2] Daniel Schultz,[2] and Carey D. Nadell[1,2,3,*]
[1]Department of Biological Sciences, Dartmouth College, Hanover, NH 03755, USA
[2]Department of Microbiology and Immunology, Geisel School of Medicine at Dartmouth College, Hanover, NH 03755, USA
[3]Lead contact
*Correspondence: carey.d.nadell@dartmouth.edu
https://doi.org/10.1016/j.cub.2024.07.078

SUMMARY

Despite competition for both space and nutrients, bacterial species often coexist within structured, surface-attached communities termed biofilms. While these communities play important, widespread roles in ecosystems and are agents of human infection, understanding how multiple bacterial species assemble to form these communities and what physical processes underpin the composition of multispecies biofilms remains an active area of research. Using a model three-species community composed of *Pseudomonas aeruginosa*, *Escherichia coli*, and *Enterococcus faecalis*, we show with cellular-scale resolution that biased dispersal of the dominant community member, *P. aeruginosa*, prevents competitive exclusion from occurring, leading to the coexistence of the three species. A *P. aeruginosa bqsS* deletion mutant no longer undergoes periodic mass dispersal, leading to the local competitive exclusion of *E. coli*. Introducing periodic, asymmetric dispersal behavior into minimal models, parameterized by only maximal growth rate and local density, supports the intuition that biased dispersal of an otherwise dominant competitor can permit coexistence generally. Colonization experiments show that WT *P. aeruginosa* is superior at colonizing new areas, in comparison to *ΔbqsS P. aeruginosa*, but at the cost of decreased local competitive ability against *E. coli* and *E. faecalis*. Overall, our experiments document how one species' modulation of a competition-dispersal-colonization trade-off can go on to influence the stability of multispecies coexistence in spatially structured ecosystems.

INTRODUCTION

Many microbes encounter and interact with solid-liquid and air-liquid interfaces[1] to which they may attach and embed themselves in a secreted polymer matrix to form biofilms.[2–8] This mode of growth entails fundamentally distinct elements of spatial competition and interactive behavior relative to planktonic growth.[9] Biofilm formation inherently involves a struggle for limited space and nutrients,[10] and as examples of microscopic ecosystems containing multiple strains and species, natural biofilms are expected to emerge from a mixture of mutually helpful, competitive, and actively antagonistic cell-cell interactions.[11] Given that space and growth substrates can quickly become scarce among tightly packed multispecies groups of bacteria, how do multiple genotypes coexist despite the prevailing impact of competition?[10,12–18] More specifically, how does the behavior of microbes in biofilm contexts influence coexistence among different microbial strains and species in manners distinct from those that occur in liquid conditions? These are core questions for the general ecology of microbial biofilm formation.

Ecological theory predicts that for *N* genotypes (different strains and species) to coexist in an ecosystem, they must be constrained by at least *N*-independent limiting factors. These limiting factors can be resource types, interactions within and among species, and myriad environmental features.[19–25] When an ecosystem varies in space or time, the number of limiting factors can increase, and additional genotypes can coexist in the heterogeneous ecosystem, when otherwise they would be lost in a corresponding homogeneously mixed system.[24,26] While this theory does not necessarily predict specific mechanisms that drive coexistence for every instance, it provides an overarching framework that can aid in looking for specific mechanisms. The physiological details of biofilm formation vary substantially between different species, but most examples are heterogeneous in time and space in terms of solute and matrix composition and cellular physiology.[2,27,28] Biofilm structure systematically changes through time as cells alter their metabolic activity, secrete adhesins, and regulate many other phenotypes during cell group growth. Additionally, mechanical interactions within and among biofilm cell groups and the depletion of local resource solutes generate gradients of key resources that often feed back to community dynamics, and vice versa.[16,29–32]

Although we have extensive documentation of heterogeneity of biofilm architecture and cell physiology in time and space, there is at present minimal exploration of how biofilm-specific behavior influences multispecies coexistence and how these details may be distinct from principles that operate in well-mixed liquid environments. Of the work that has studied the stability of multi-strain and multispecies coexistence in biofilms, little

Please cite this article in press as: Holt et al., Dispersal of a dominant competitor can drive multispecies coexistence in biofilms, Current Biology (2024), https://doi.org/10.1016/j.cub.2024.07.078

has measured biofilm structure at the resolution of individual cells. This cellular-scale quantitative perspective can add new insight into how individual cell behavior and physiology translate to higher-order group structure and composition.[33,34]

Here, we developed a model biofilm community composed of *Pseudomonas aeruginosa*, *Escherichia coli*, and *Enterococcus faecalis*. All three bacterial species can behave as opportunistic pathogens and are frequently isolated from catheter-associated urinary tract infections.[35–37] Our core goal was to determine how these three species assemble to form a community and what mechanisms unique to the biofilm mode of life influence the community's steady states. To accomplish this, we used a combination of liquid shaking culture, microfluidic culture, confocal microscopy, cellular resolution image analysis, and minimal mathematical models. In well-mixed liquid culture experiments, we found that coexistence does not occur among all three species; *P. aeruginosa* displaces the other two. In biofilm culture on submerged surfaces, however, we did observe coexistence of all three species for as long as we ran the experiment (up to 25 days), with *P. aeruginosa* in the majority. We observed that *P. aeruginosa* undergoes cycles of mass dispersal that drive accompanying fluctuations in biofilm community size and cell packing architecture. By manipulating the ability of *P. aeruginosa* to disperse, using a targeted gene deletion, we found that these mass-dispersal events are a key driver of localized three-species coexistence in our model biofilm system. Simple models illustrate how the observed mass-dispersal dynamics can lead to stable coexistence in a spatial setting, so long as *P. aeruginosa* is dispersing in greater proportion to its starting population size than the other two species. Dispersal-deficient *P. aeruginosa* has increased local competitive ability within multispecies biofilms and drives out *E. coli* entirely, but it is substantially deficient in its per-cell dispersal and colonization of other locations. Taken together, our results illustrate how one species' competition/dispersal/colonization trade-off can cause temporal fluctuations in microscopic biofilm ecosystems and drive localized coexistence among different species.

RESULTS

P. aeruginosa, *E. faecalis*, and *E. coli* can cohabitate over multiple weeks in biofilms

P. aeruginosa, *E. faecalis*, and *E. coli* were engineered to constitutively produce the fluorescent proteins mKO-κ, GFP, and mKate2, respectively, such that they could be distinguished by live-cell fluorescence microscopy. The three species were inoculated at a 1:1:1 ratio either in shaken liquid culture or into microfluidic devices composed of poly-dimethylsiloxane (PDMS) chambers bonded to glass coverslips. For biofilm experiments, after a 1-h attachment period, the species were incubated under continuous flow of 1% tryptone broth medium for up to 350 h at 0.05 μL/min (average flow velocity ~ 23.4 μm/s). As a proxy for population size, the total biovolume of each species was measured by confocal microscopy at 24-h intervals and used to calculate relative abundance. We found that the three species could cohabitate to form a biofilm community (Figures 1A and 1B), which occurred despite high variance in community composition at initial time points (Figures 1B–1D and S1). For liquid culture experiments, strains were inoculated at a 1:1 ratio in identical media conditions, incubated with shaking, and transferred 1:100 to fresh medium every 24 h. The consistent cohabitation of all three species was specific to the microfluidic biofilm environment: in our shaken liquid culture experiments, *P. aeruginosa* displaced *E. coli* and *E. faecalis* from the system (Figure 1A). This discrepancy in outcome between the biofilm and planktonic culture experiments suggests that the spatial constraints and/or the specific physiological states of the species in the biofilm mode of life play an important role in these three species' ability to cohabitate within the microfluidic flow environment. The results of dual culture experiments follow the same trends, with cohabitation occurring in biofilm culture but not in planktonic culture. For the pairing of *E. coli* with *E. faecalis*, we observe cohabitation in both biofilm and planktonic culture conditions, consistent with prior work on the interaction of these two species (Figures S2–S4).[38]

To determine the nature of the primary ecological relationship between the three species, we measured the biovolume of each species across the first 96 h of growth under two conditions: three-species co-culture, two-species co-culture, and single-species monoculture. We found that the biovolume and therefore population size of each species is higher in monoculture than in tri-culture or dual culture over this time frame, indicating that the three species are primarily competing with one another in the biofilm context used here (Figures 1C and S2–S5).

Inspecting the image data in more detail reveals interesting patterns that begin to indicate what kinds of biofilm-specific behavior may be contributing to apparent coexistence in the full three-species system. For the example time series shown in Figure 1E, we note that the biofilm community is first dominated by *E. faecalis* and *E. coli* at early time points, followed by rapid growth of *P. aeruginosa*, which partially displaces the other two species. After reaching high densities, there is a widespread and rapid decline in *P. aeruginosa* volume and what appears to be an increase in relative abundance of the other two species. The same cycle of *P. aeruginosa* population expansion and then contraction occurs once again before the time series is halted. It is notable that despite high variance in the initial attachment of the three species across many runs of the experiment, the driving pattern of *P. aeruginosa* population growth and precipitous decline was consistent across all replicates. We attribute the variance in the three species' initial attachment (and therefore starting ratio) to random noise in surface conditions within our chambers, adhesin expression physiology among cells of the three species, and reversible attachment behavior during early biofilm formation.[8,39–41] *P. aeruginosa* dispersal behavior has been studied in considerable detail and is known to depend on rhamnolipid secretion, responses to the local environment, and responses to self.[42–48] It has previously been reported that *P. aeruginosa* monocultures grown in microfluidic chips experience rhamnolipid-dependent self-induced dispersal events, and we have recapitulated this result in our conditions (Figure S6).[49–51] We speculated on the basis of these results and prior literature that *P. aeruginosa* was actively dispersing from the chambers after reaching large enough group sizes; it also appeared that the dispersal process was biased in the sense that *P. aeruginosa* departs the biofilm chambers in proportionally greater numbers relative to its resident biofilm population size in comparison with the other two species (Figure 1E). In the

Please cite this article in press as: Holt et al., Dispersal of a dominant competitor can drive multispecies coexistence in biofilms, Current Biology (2024), https://doi.org/10.1016/j.cub.2024.07.078

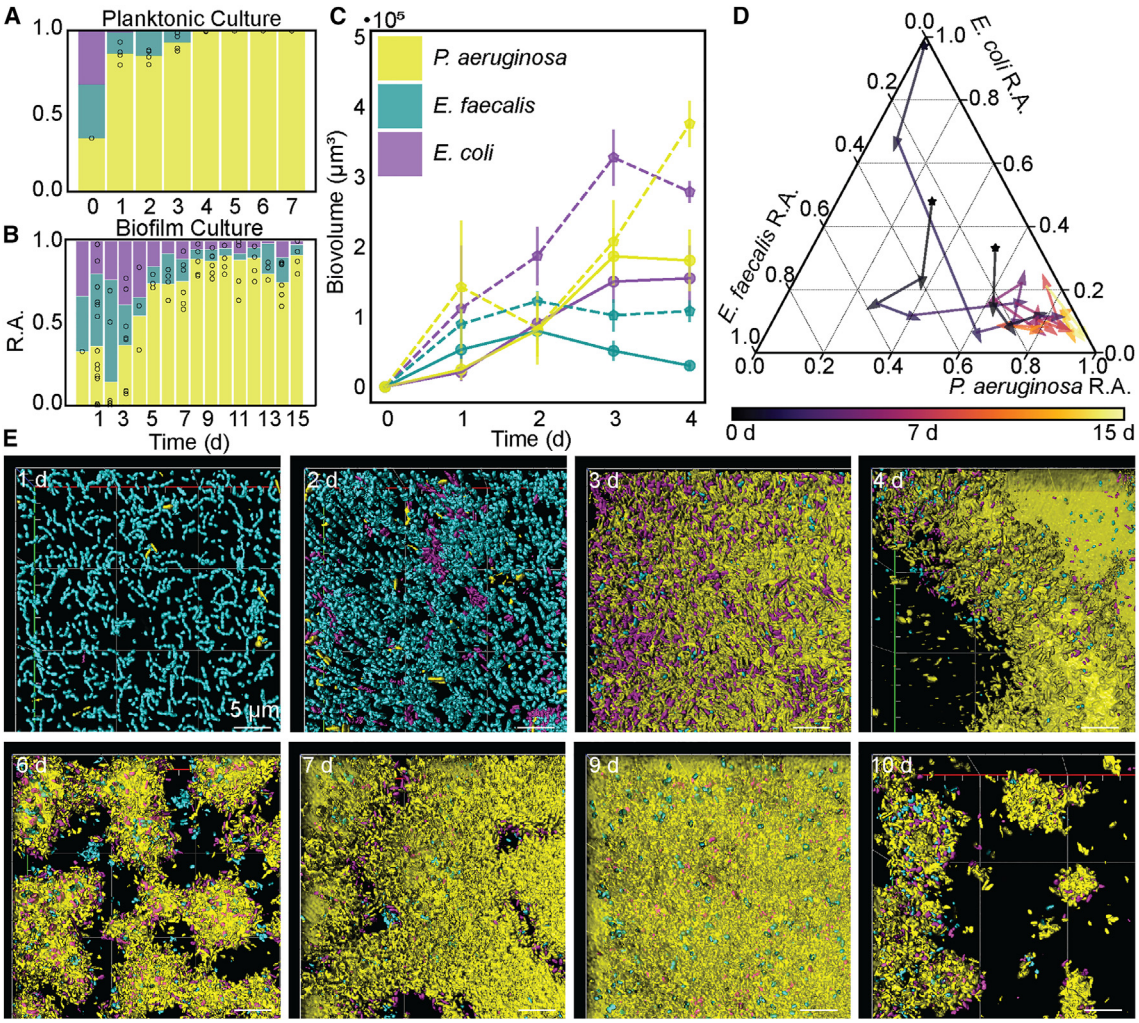

Figure 1. *P. aeruginosa* (yellow), *E. faecalis* (cyan), and *E. coli* (purple) appear to coexist in biofilm communities despite prevailing competition between them

(A) Relative abundances of the three species in planktonic culture (n = 4 per time point).

(B) Relative abundances of the three species in biofilm culture (n = 3–12 per time point).

(C) Measurement of each species' biovolume in a 212 × 212 μm field of view during monoculture (dashed line) and co-culture (solid line) biofilms. Dots represent the mean, and error bars represent standard error (n = 3–12 per time point).

(D) Ternary plot relative abundance trajectories from three independent biofilm replicates colored by time.

(E) Representative 3D renderings of the three species growing in a biofilm over time (n = 3 trajectories from independent experiments).

See also Figures S1–S5.

following section, we use simple mathematical models to assess how different dispersal regimes might contribute to long-term cohabitation, and we compare modeling results with experiments to determine which of these dispersal regimes provides the best fit to our *in vitro* biofilm experiments.

Density-dependent, biased dispersal of a competitively dominant species can permit coexistence with other species in the biofilm context

Our exploratory experiments above indicated that the biofilm environment can allow for cohabitation among *P. aeruginosa*, *E. coli*, and *E. faecalis*, whereas the planktonic environment does not. We also documented that dispersal events occur in biofilm environments and that they appear to be controlled by *P. aeruginosa*, leading to preferential removal of *P. aeruginosa* from the system. We speculated that this dispersal process, by generating negative density dependence on the rate of change in *P. aeruginosa* abundance, may be particularly important as a biofilm-specific phenomenon contributing to multispecies coexistence.[25,26,52–55] Before proceeding with further analyses and experiments, we sought to verify that this idea is valid in principle by using simple modeling approaches.

We explored in particular how different dispersal regimes may influence the propensity for three species to coexist in a local environment, parameterizing the system using the relative maximal growth rate and carrying capacity (mean local biovolume density) for each species, extracted from our experiments in the previous section (Figures 1C and S5; STAR Methods). Specifically, we

Please cite this article in press as: Holt et al., Dispersal of a dominant competitor can drive multispecies coexistence in biofilms, Current Biology (2024), https://doi.org/10.1016/j.cub.2024.07.078

implement a growth scenario in which no dispersal occurs, another in which unbiased dispersal occurs and removes each species by equal fractions, and finally a biased dispersal condition in which *P. aeruginosa* disperses in a substantially larger fraction relative to *E. coli* and *E. faecalis*.

The different dispersal scenarios noted above are based on the distinct mechanisms of biofilm dispersal regulation that have been genetically characterized in the literature.[8,42,43,50,56–58] In the absence of dispersal, our experimentally derived model parameters predict that *P. aeruginosa* will displace both of the other two species (Figure 2A). We sought to explore unbiased dispersal because *P. aeruginosa* rhamnolipids, used as a surfactant during active dispersal, are known to be capable of dispersing biofilms formed by other species as well (Figure 2B).[49,51,59,60] Additionally, if *E. coli* and *E. faecalis* are embedded within dispersing *P. aeruginosa* biomass, then it is conceivable that they too could be dispersed due to their spatial arrangement. Furthermore, we were also interested in the case where dispersal events are biased toward removing *P. aeruginosa* (Figure 2C). This could happen if the biofilm locations that disperse are disproportionally dominated by *P. aeruginosa*, which appeared to be the case by visual inspection of our image data in the previous section (Figures 1E, 2D, and S4).

In brief, we find that implementing biased dispersal of *P. aeruginosa* in a density-dependent manner can stabilize the community such that all three members coexist, while unbiased or no dispersal of *P. aeruginosa* cannot support all three members locally coexisting. This result is specific to the spatial stochastic model and does not hold when the stochastic-spatial system is randomly mixed at each time step (Figure S7). We systematically assessed the stability of coexistence in the case of biased dispersal, finding that when dispersal is sufficiently biased toward the dominant biofilm competitor, the system will converge to a dynamic equilibrium of coexistence from any starting ratio of the three species in the system (Figure 3). Moreover, each of the three species can invade from rarity into a system containing only the other two species (this result is confirmed experimentally in the following sections) (Figure S7). The three species' mutual invasibility reinforces the conclusion of stable coexistence by indicating that if one species were to go locally extinct, it could re-invade from rarity so long as there is a source of incoming dispersed cells from elsewhere (i.e., so long as the species that became locally extinct did not also become globally extinct). By varying the dispersal ratio from biased (ratio of 0) to unbiased (ratio of 1) and varying the relative fitness of *P. aeruginosa* from low to high in the stochastic-spatial model, one can visualize the relationship between *P. aeruginosa* relative fitness and the magnitude of dispersal bias needed to maintain coexistence (Figures 2E–2H).

For consistency with the historical literature, we also implemented mean-field and reaction-diffusion models of our three-species system. These models are a poorer representation of the system because of their assumptions of continuous time (and space, for the reaction-diffusion model), but generally, they support the core logic of our lattice model results (Figure S8).

We note that our results are distinct from the well-explored connection between coexistence in multi-patch systems through a competition-colonization trade-off, where all species experience a strict negative relationship between local competitive ability and dispersal/colonization ability.[25,61–67] Our modeling work here focuses on and supports the simple intuition that one competitively dominant species, if it regularly disperses without carrying significant amounts of the other two species with it, can permit stable coexistence with other less locally competitive species.[25,52,53,68] This occurs because the dispersal events selectively lower the time-averaged abundance of the stronger competitor, giving the other species space and time to replicate sufficiently to maintain a positive population size. Even though our community dynamics data may give the impression of negative frequency-dependent selection, this is not quite the case, either: *P. aeruginosa* does not have a fitness disadvantage when it reaches high relative abundance. Rather, at high density it simply removes a substantial fraction of its own cell count from the local population in order to disperse elsewhere.

The modeling results and experimental observations above led us to speculate that when dispersal events occur in long-lived biofilms of *P. aeruginosa*, *E. coli*, and *E. faecalis*, these events are driven by *P. aeruginosa*, and *P. aeruginosa* is removed from the system in greater proportion to its resident biofilm population size. We directly tested this idea by quantifying the population dynamics of each species in relation to changes in *P. aeruginosa* local abundance within the three-species system. Using the time course data from our 350 h experiments, we calculated the change in each species' biovolume—which again here is a proxy for population size—as a function of the change in the biovolume of only *P. aeruginosa* in the time following dispersal events. This analysis was consistent with our hypothesis that *P. aeruginosa* dispersal events are primarily removing *P. aeruginosa* from the system. As anticipated, the *P. aeruginosa* time-averaged rate of population change is positive when it is at low density and negative when it is at high density, and this trend is similar both in monoculture and co-culture (Figures 2E and S9A). This latter point emphasizes that *P. aeruginosa* is driving its own dispersal dynamics mostly or completely independently of the presence of the other two species. Additionally, the per day changes in abundance of *E. coli* and *E. faecalis* are only weakly correlated with the per day change in abundance of *P. aeruginosa*. This quantification reinforces our intuition from the previous section and suggests that during mass-dispersal events, it is primarily *P. aeruginosa* that is departing the system (Figures 2F and S9B).

We did note that the correlation between declines in *E. faecalis* and *P. aeruginosa* was statistically significant if minor in terms of magnitude. We wondered why this might be the case and began by exploring the spatial relationship between the three species. We noted that while *E. coli* and *E. faecalis* tended to be found around the periphery of *P. aeruginosa* cell groups, only *E. faecalis* could also be found in the middle of *P. aeruginosa* cell groups. We could confirm this visual intuition quantitatively by measuring the spatial occurrence of *E. coli* and *E. faecalis* in relation to the local density of *P. aeruginosa*, as well as by calculating the distance to the closest neighbor for each species pairing (Figures 2G and 4). These observations are consistent with the explanation that the portion of *E. faecalis* population found within *P. aeruginosa* cell groups is driving the correlation between declines in *P. aeruginosa* and *E. faecalis*.

Please cite this article in press as: Holt et al., Dispersal of a dominant competitor can drive multispecies coexistence in biofilms, Current Biology (2024), https://doi.org/10.1016/j.cub.2024.07.078

CellPress

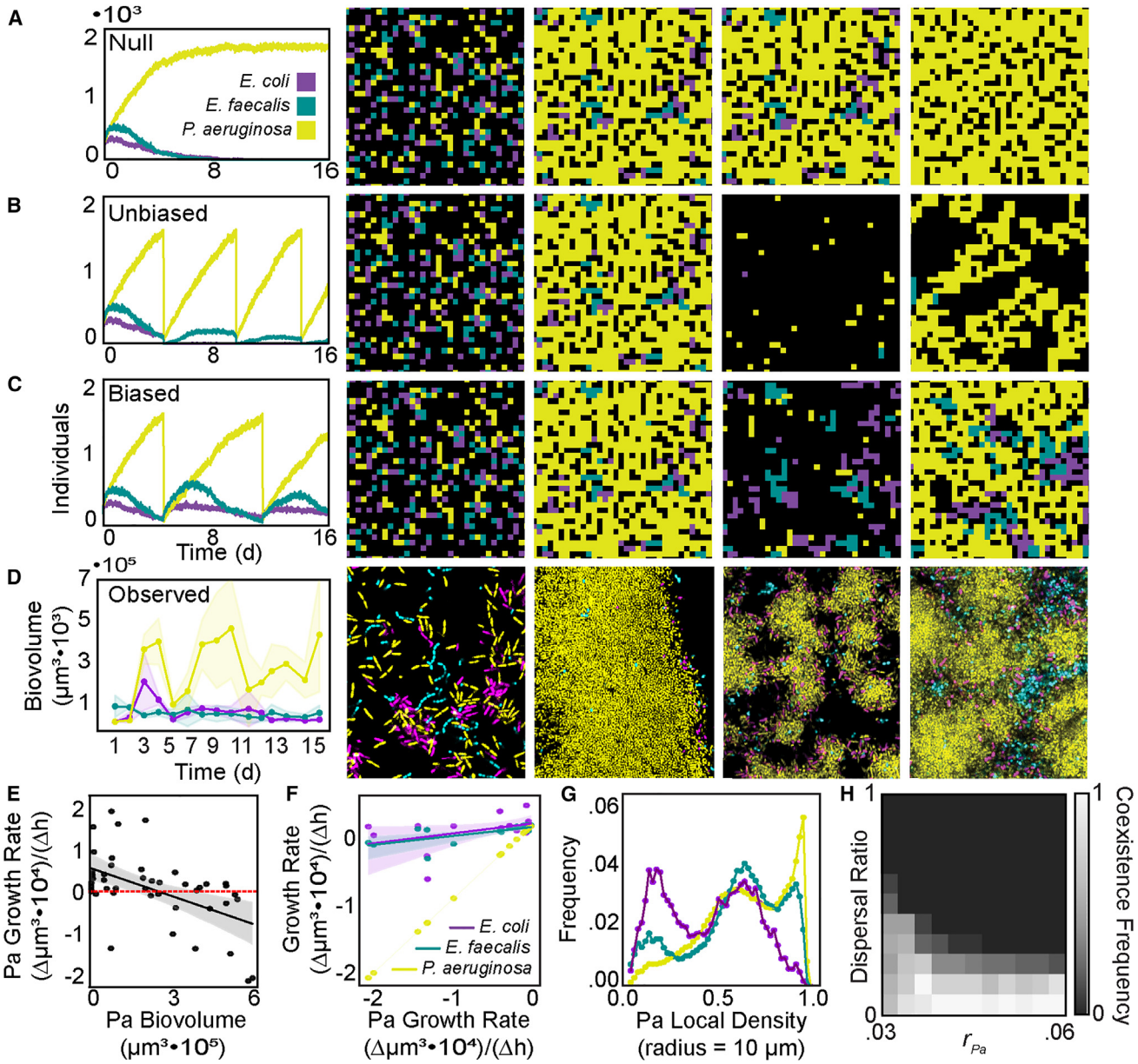

Figure 2. Minimal models and experimental data support dispersal as a mechanism of coexistence

(A) Population dynamics and images of the no-dispersal case from the stochastic-spatial model.

(B) Population dynamics and images of the unbiased dispersal case from the stochastic-spatial model.

(C) Population dynamics and images of the biased dispersal case from the stochastic-spatial model.

(D) Representative population dynamics and images from the biofilm experimental dataset (one experimental run is shown here with the variance around each line derived from three technical replicates).

(E) Linear regression of *P. aeruginosa* biovolume against *P. aeruginosa* growth rate ($r^2 = 0.25$, $p = 0.0002$, $n = 3$).

(F) Linear regression of negative *P. aeruginosa* growth rate against the growth rate of the other species. *E. coli* does not correlate (purple, $r^2 = 0.16$, $p = 0.0979$, $n = 3$). *E. faecalis* correlates moderately (cyan, $r^2 = 0.49$, $p = 0.0037$, $n = 3$).

(G) *P. aeruginosa* local density (r = 10 μm) as a frequency of total biomass ($n = 4$).

(H) Phase diagram of model outcomes for long-term coexistence as the dispersal ratio (δ_i/δ_{Pa}) is varied from only *P. aeruginosa* dispersing to all species dispersing in equal proportions (dispersal ratio of 1), and *P. aeruginosa* growth rate (r_{Pa}) is varied from 0.03 to 0.06.

See also Figures S4–S9 and Table S1.

All told, our data support the interpretation that mass-dispersal events are driven primarily by *P. aeruginosa* in a density-dependent manner and that because of the spatial relationships among the three species, *E. coli* and *E. faecalis* are much less likely than *P. aeruginosa* to depart the system during these dispersal events. Our modeling supports the inference

Please cite this article in press as: Holt et al., Dispersal of a dominant competitor can drive multispecies coexistence in biofilms, Current Biology (2024), https://doi.org/10.1016/j.cub.2024.07.078

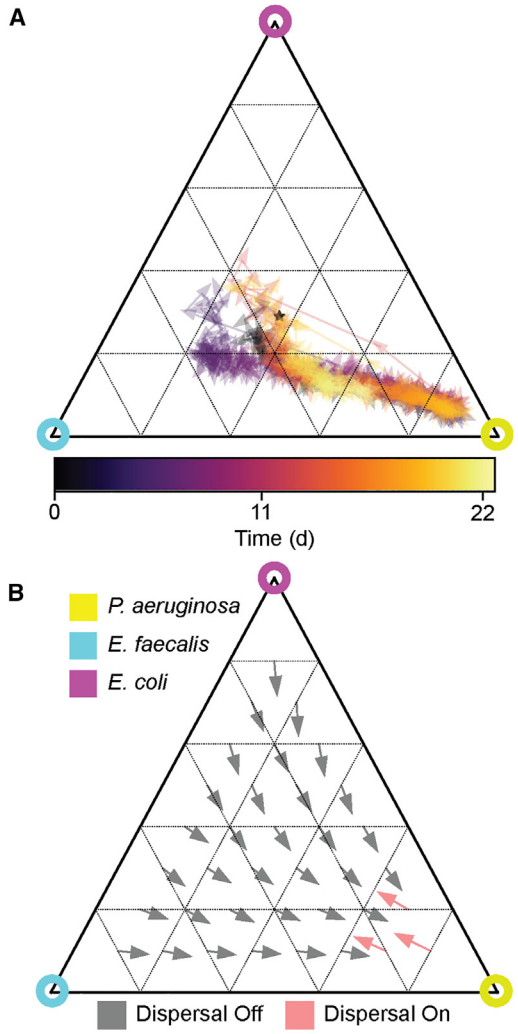

Figure 3. Vector plot analysis of the biased dispersal stochastic-spatial model supports long-term coexistence

(A) Representative trajectory of a single run showing multiple cycles of dispersal.

(B) Average vectors from 400 individual simulation runs show that the three species are maintained over time.

See also Figures S5 and S7.

that biased dispersal of an otherwise dominant biofilm competitor can drive coexistence on its own; this idea, although simple in principle and robustly supported by our modeling work, requires careful experimentation to confirm. In the following sections, we explore in greater detail the correspondence between our experimental system and the abstraction of the modeling work, and we consider the effects of dispersal behavior on competition at larger spatial scales involving multiple resource patches.

A *P. aeruginosa* mutant with reduced dispersal does not permit local three-species coexistence

To assess the idea that cyclic dispersal of *P. aeruginosa* is necessary for the coexistence observed in our three-species biofilm community model, we generated a *P. aeruginosa* strain with reduced dispersal relative to the parental wild-type (WT) PA14. Specifically, we produced a strain harboring a clean deletion of *bqsS*, which encodes the transmembrane sensor of the BqsR/BqsS two-component system that responds to Fe(II) concentration.[69] One of the primary phenotypes of a *bqsS* deletion mutant is strongly reduced biofilm dispersal, caused at least in part by a significant decrease in the production of surfactants and proteases.[47,70,71] Thus, this mutant afforded an opportunity for testing the effects of reduced biofilm dispersal by *P. aeruginosa* on multispecies biofilm community dynamics in co-culture with *E. coli* and *E. faecalis*. Other mutants of *P. aeruginosa*, for example, those defective for rhamnolipid production, are also dispersal deficient. We chose the *bqsS* deletion mutant as representative of a minimally dispersing strain, because it is the only example (to our knowledge) that has few, if any, other pleiotropic effects on cell-cell interaction in the context of multispecies competition.

We first took note of the obvious architectural differences between biofilms containing WT *P. aeruginosa* in comparison with the Δ*bqsS* derivative. While WT *P. aeruginosa* biofilms are heterogeneous and harbor regions with lower local density, Δ*bqsS* biofilms are skewed toward higher local density (Figures S10 and S11). This architectural difference was maintained in the three-species biofilms, where WT PA14 displayed regions of high-density *P. aeruginosa* (which permitted little of the other two species to enter) and other lower-density regions in which all three species were observed (Figures 5A, S10, and S11). Biofilms containing Δ*bqsS P. aeruginosa* appeared to contain almost exclusively high-density regions of the Δ*bqsS* mutant, with few detectable cells of the other species (Figures 5A, S10, and S11). Quantification of relative abundance of *P. aeruginosa* in the two conditions confirmed these observations: the Δ*bqsS* mutant rose to nearly 100% of the community in most locations and replicates of the experiment, while WT *P. aeruginosa* stabilized at ∼85%, as observed above (Figure 5B). Notably, averaged over all runs of the experiment, the Δ*bqsS* deletion mutant accumulated nearly double the total biovolume over the course of biofilm growth relative to the WT PA14 parental strain (Figure 5C). These data are all consistent with the hypothesis that the Δ*bqsS* mutant disperses less than its parental strain and that its decreased or eliminated dispersal reduces the ability of the three species to cohabit a patch of biofilm growth on the sub-millimeter scale.

A useful criterion for coexistence of a given set of species is that they can each increase in abundance when rare in the community.[25] An effective test of this criterion is to determine if each species can invade the community, that is, propagate to stable positive population size from initial rarity.[25,72,73] The rationale for this test is that if all the constituent species of a community can re-invade when rare, then over the long term, all species in the community will persist together in a dynamically stable, if not necessarily static, equilibrium. Thus far, we have been measuring the population dynamics of *P. aeruginosa*, *E. coli*, and *E. faecalis* from 1:1:1 starting inoculations. To conclude this section, we sought to test the strict coexistence criterion that each species can invade biofilms composed of the other two. We did this by growing two-species biofilms for each potential combination of the three species for 96 h, followed by a pulse of the third "invader" species over the course of 2 h. This full set of invasion experiments was performed with both the WT PA14

Please cite this article in press as: Holt et al., Dispersal of a dominant competitor can drive multispecies coexistence in biofilms, Current Biology (2024), https://doi.org/10.1016/j.cub.2024.07.078

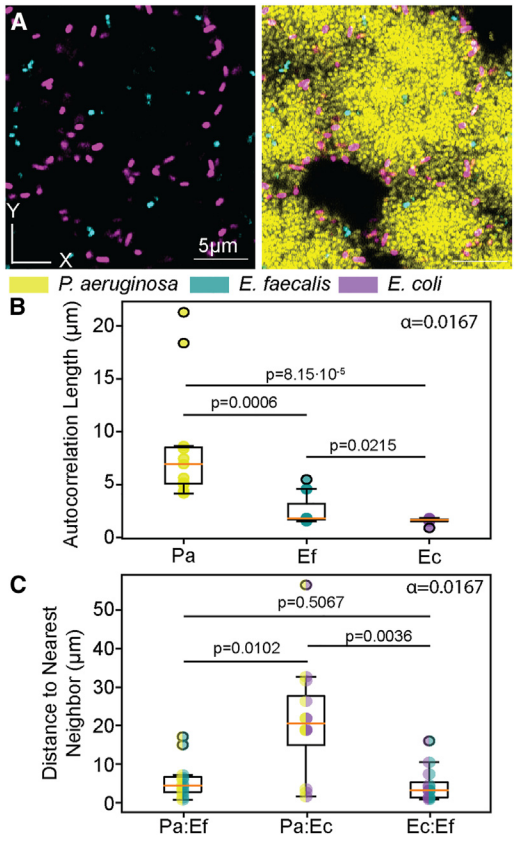

Figure 4. Spatial patterning of the three species relative to themselves and one another

(A) Representative image of the biofilm community. *P. aeruginosa* is shown in yellow, *E. coli* is shown in purple, and *E. faecalis* is shown in cyan.

(B) Autocorrelation length of each of the three species in the community at 15 days (Mann-Whitney U tests, Bonferroni corrected α, $n = 11$ locations from 3 biofilm chambers).

(C) Distance to nearest neighbor in the community at 15 days (Mann-Whitney U tests, Bonferroni corrected α, $n = 11$ locations from 3 chambers).

background and the Δ*bqsS P. aeruginosa* deletion mutant. Figure 3D illustrates that each of the three species, on average, registers positive and stable population sizes after colonizing a preexisting biofilm of the other two species when *P. aeruginosa* is WT (Figures 3E and S12). With the Δ*bqsS* strain, *E. faecalis* retains the ability to invade, but now *E. coli* cannot, illustrating that the strongly reduced dispersal phenotype of the Δ*bqsS* strain interferes with coexistence of the three species (Figures 5D and S12).

The local competitive advantage of *P. aeruginosa* Δ*bqsS* trades off against the ability to disperse to other locations

The results reported above indicate that the repeated mass-dispersal behavior of WT *P. aeruginosa* PA14 decreases its time-averaged abundance on a local scale and opens space sufficiently often to permit coexistence with *E. coli* and *E. faecalis*. The Δ*bqsS* deletion mutant of *P. aeruginosa*, whose dispersal is substantially reduced, does permit coexistence with *E. faecalis*, albeit with *E. faecalis* at very low population size, but not with *E. coli*, which is no longer able to invade a resident biofilm of the two other species. We hypothesized that WT *P. aeruginosa*, although unable to displace the other two species locally, may be balancing a trade-off between local competition and dispersal to other locations relative to the growth behavior of a Δ*bqsS* mutant. The rationale for this hypothesis is that there is a fundamental limitation on the total accumulation of cells produced by each species' growth and division. Cells may stay in place and contribute to local competition, or they may disperse into the liquid phase and perhaps find new locations elsewhere to inhabit. Our parental strain of *P. aeruginosa* accumulates biomass locally and then disperses a large fraction of these cells into the liquid dispersal phase when it reaches high local population density. The Δ*bqsS* mutant, by contrast, reduces its investment into the dispersal pool and instead remains primarily in place, devoting more mass and energy to local competition versus dispersal to new locations.

We sought to test this possibility by comparing the relative local population growth and dispersal of WT versus Δ*bqsS* PA14, noting that the Δ*bqsS* mutant does accumulate greater biomass locally than the WT strain (Figure 6A). When the effluent from chambers containing these two different strains of *P. aeruginosa* (growing in co-culture with *E. coli* and *E. faecalis*) was used to colonize new microfluidic devices, however, the WT strain of PA14 showed substantially higher colonization, including deposition of large groups of cells, which had been either released from the upstream chamber as dispersing cell groups or formed by aggregation after arriving in the new chamber. This rapid formation of the three-dimensional biofilm structure is likely advantageous in environments containing exogenous threats such as bacteriophage and predators.[74–80] Additionally, these cell groups were consistent in spatial arrangement and composition of the three species within the original upstream biofilms containing WT *P. aeruginosa*, suggesting a continuation of coexistence across patches. The Δ*bqsS* mutant, by contrast, was slower to colonize downstream chambers, consistent with the idea that its local competitive advantage carried a cost of decreased ability to disperse and colonize other locations distal to the focal patch in which biofilm growth was occurring (Figures 6B–6D).

DISCUSSION

Using microfluidic culture methods, we generated a model three-species biofilm community composed of *E. coli*, *E. faecalis*, and *P. aeruginosa*, which we found can coexist with one another. Coexistence of the three species, each of which can invade the other two from rarity to a positive population size, is specific to biofilm culture conditions: in shaken liquid culture, *P. aeruginosa* competitively displaces the other two species. We found that three-species coexistence depends on cyclic mass dispersal that is primarily driven by *P. aeruginosa*, which recapitulates similar cycling of dispersal and regrowth in biofilm culture on its own. Via this pattern of repeated dispersal, *P. aeruginosa* lowers its time-averaged abundance and generates variance in proportion of space occupancy over time, which is a key factor allowing the other

Please cite this article in press as: Holt et al., Dispersal of a dominant competitor can drive multispecies coexistence in biofilms, Current Biology (2024), https://doi.org/10.1016/j.cub.2024.07.078

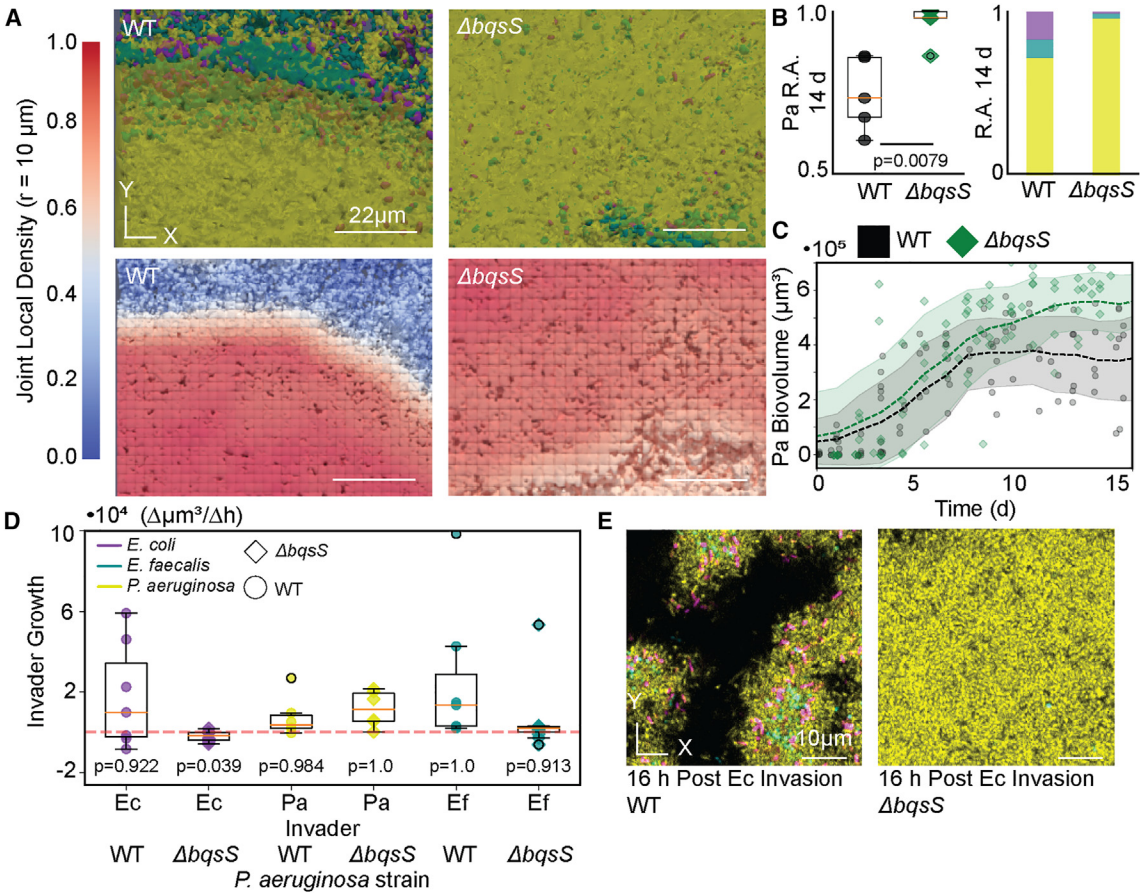

Figure 5. *P. aeruginosa ΔbqsS* has increased biofilm local density and invasion resistance

(A) 3D renderings of *P. aeruginosa* WT and Δ*bqsS* biofilms and corresponding joint local population density measurement (r = 10 μm). *P. aeruginosa* is shown in yellow, *E. coli* is shown in purple, and *E. faecalis* is shown in cyan.

(B) Box-and-whisker plots showing that *P. aeruginosa* WT has significantly lower relative abundance in the three-species community relative to the *ΔbqsS* mutant (Mann-Whitney U test, $n = 5$).

(C) Time-averaged trajectories of WT *P. aeruginosa* and *ΔbqsS* biovolume in the biofilm community. Dashed lines represent the time-averaged mean (3 days window), and the shaded region represents one standard deviation above and below the time-averaged mean ($n = 3$–10).

(D) Box-and-whisker plots of single-species growth after invasion into a two-species biofilm showing that *E. coli* cannot invade the *ΔbqsS-E. faecalis* biofilm (Wilcoxon tests against null that data fall above zero, $n = 6$–10).

(E) Representative images of the invasion of *E. coli* into a 96-h biofilm composed of *E. faecalis* and *P. aeruginosa*.

See also Figures S10–S12.

two species to coexist with it on a local scale. These inferences from the experimental results were robustly supported by stability and invasion analyses of our corresponding stochastic-spatial lattice model. A Δ*bqsS* mutant of *P. aeruginosa*, whose dispersal is far reduced relative to the parental PA14, still permits cohabitation with *E. faecalis* but drives *E. coli* locally extinct. However, the same Δ*bqsS* mutant has considerably lower ability to colonize new locations elsewhere relative to WT *P. aeruginosa*. These results highlight the ability of biofilm dispersal/competition trade-offs to shape microbial community composition across single- and multi-patch spatial scales.

Our experimental results are consistent with long-standing ecological theory establishing that both temporal and spatial heterogeneity can create additional factors that limit different species' abundance.[24,26] Using detailed image analysis, we find that in our experimental system, *P. aeruginosa* dispersal creates a heterogeneous biofilm architecture that underlies *E. coli*'s ability to coexist in the community. Numerous physical and biological mechanisms through which the biofilm mode of life generates variation among the cells dwelling within have been identified and characterized.[30,81] However, the extent to which these biofilm-specific features generate additional limiting factors pertinent to multispecies coexistence, allowing biofilms to support greater numbers of species than well-mixed environments, has received much less attention.[82,83]

Here, we have shown in detail that one specific type of biofilm behavior, active dispersal of a single dominant species, can increase the number of species that a biofilm can support. This occurs because biased dispersal decreases the dispersing species' time-averaged rate of change in population size and generates both spatial and temporal heterogeneity in the local biofilm ecosystem. Density-dependent

Please cite this article in press as: Holt et al., Dispersal of a dominant competitor can drive multispecies coexistence in biofilms, Current Biology (2024), https://doi.org/10.1016/j.cub.2024.07.078

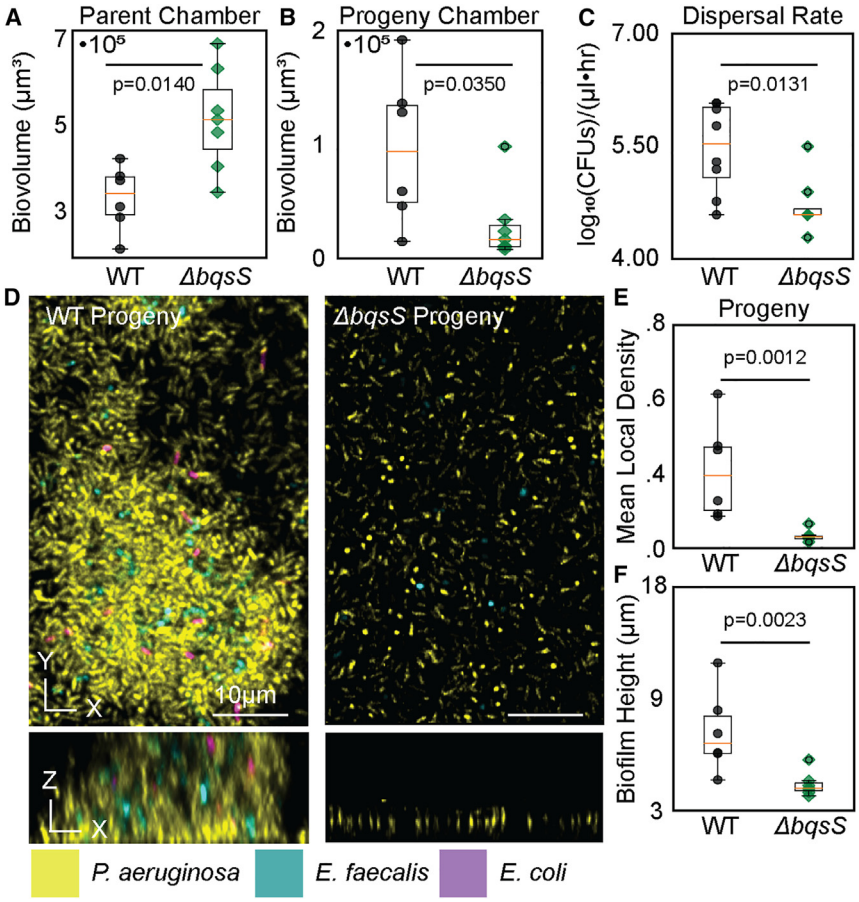

Figure 6. A *P. aeruginosa bqsS* deletion mutant has a lower dispersal rate and decreased colonization ability in comparison with *P. aeruginosa* WT

(A) Box-and-whisker plots showing significantly higher biovolume in the *ΔbqsS P. aeruginosa* parent/seeding chamber relative to WT (Mann-Whitney U test, $n = 6$).

(B) Box-and-whisker plot showing significantly less *ΔbqsS* biovolume in the colonized chamber relative to WT (Mann-Whitney U test, $n = 6$ chambers).

(C) Box-and-whisker plots showing a significant difference in CFU dispersal rates between WT and *ΔbqsS* (Mann-Whitney U test, $n = 7$).

(D) Representative images of WT and *ΔbqsS* colonizing a sterile progeny chamber. *P. aeruginosa* is shown in yellow, *E. coli* is shown in purple, and *E. faecalis* is shown in cyan.

(E) Box-and-whisker plots showing that the WT, mean, joint, local density ($r = 10$ μm) is significantly higher within the newly colonized chamber (Mann-Whitney U test, $n = 6$).

(F) Box-and-whisker plots showing that the biofilm height (μm) of WT is significantly higher within the newly colonized chamber (Mann-Whitney U test, $n = 6$).

See also Figure S12.

dispersal is just one of many forms that dispersal from a biofilm can take, which should be noted. Dispersal from a biofilm can occur as a passive result of physical forces, an active response to environmental signals, or as an active response to self-created signals.[6,8,27,28,43,56,57] Whole sections or subsections of biofilms growing under shear stress can be removed *en masse* in what are often referred to as sloughing events. Less drastically, the growing edge of a biofilm often loses population members continuously, although in lower numbers relative to sloughing events, in an erosion-like process.[84] The environmental cues that drive dispersal are diverse and vary between different species, but quorum-sensing regulation and starvation response are commonly involved.[57,58,85–88] How biofilms' often high variance in structure over time and space impacts microbial ecosystem species richness remains an important direction for future work using both *in vitro* systems accessible to live time-lapse microscopy and more naturalistic systems and settings.[89–91]

Although we have identified how a cyclic dispersal process can contribute to multispecies coexistence, we cannot say for sure how other types of cell-cell interaction may underlie some of the fundamental competitive dynamics in the three-species system studied here. We did not, for example, examine the potential roles of secreted substance-based interactions, which likely account in some part for the competitive dominance of *P. aeruginosa* in the liquid culture condition and its ability to occupy the majority of the biofilm community even when it is dispersing regularly. For example, PA14 produces a copious biofilm matrix including polysaccharide, protein, and DNA components; high matrix secretion helps to explain PA14's robust biofilm growth and has been shown to contribute directly to competition for space.[92–95] *P. aeruginosa* also produces a broad array of molecular weapons—such as pyocyanin, hydrogen cyanide, tailocins, and contact-dependent type VI secretion systems, among others—all of which have been explored in some depth previously.[96–101] Some of these factors may well contribute to the baseline competitive dynamics in our experiments here, although we note that the constant flow used in our biofilm culture conditions can drastically shrink the range of influence of diffusible secreted compounds.[102] On the other hand, prior work has indicated that *E. coli* and *E. faecalis* can interact synergistically under some conditions[38,103]—*E. coli* chemotaxes to autoinducer-2 released by *E. faecalis*, for example, which can promote their co-aggregation in biofilms.[38] But we would emphasize again here that the overall primary ecological interaction we could register in all two-species and three-species conditions was competition, in which all community members' population sizes were reduced relative to monoculture conditions. Biofilms, like all ecosystems, emerge from a complex interplay of mutually helpful, competitive, and actively antagonistic interactions among their constituent members; fully disentangling how these forces combine to yield community structure, richness, and stability remains key to areas of work at the interface of *in vitro* experimental and whole-system sampling-based approaches to microbial community ecology.

Another important direction for the future will be to explore how interactions between cohabiting species or strains can alter each community constituent's dispersal behavior. In our work, we found no evidence for *E. coli* or *E. faecalis* influencing the dispersal behavior of *P. aeruginosa*, but it is plausible that strains or species could influence others' dispersal behavior through the secretion or adsorption of extracellular products. The degree to which dispersal is modulated by cross-species or cross-kingdom interactions and the ways in which these interactions influence species coexistence are important frontiers for future research that bears on fundamental microbial ecology. This topic also bears on infection scenarios in which the tendency of one species to disseminate from an initial site of a biofilm infection may depend on which other species are present as well. Our experimental conditions in this paper are most closely comparable with medical flow devices such as slow-drip catheters, and indeed these environments motivated the choice of species for our study. Interestingly, the bqsR/bqsS two-component sensor has been shown to respond to Fe(II) and not to Fe(III).[69] While the oxidation state of Fe in the host depends on the exact microenvironment, in general anerobic conditions will favor the Fe(II) state and *P. aeruginosa*-produced phenazines can reduce Fe(III) to Fe(II).[96,104,105] Altogether, this suggests a potential relevance for the biofilm dispersal state characterized here in the context of *P. aeruginosa* biofilm infections. As always, assessing the generality of our results in other realistic settings, and with other natural and clinical isolates of the microbes in question, remains a vital front for future biofilm research and microbial ecology more generally.

STAR★METHODS

Detailed methods are provided in the online version of this paper and include the following:

- KEY RESOURCES TABLE
- RESOURCE AVAILABILITY
  - Lead contact
  - Materials availability
  - Data and code availability
- EXPERIMENTAL MODEL AND STUDY PARTICIPANT DETAILS
- METHOD DETAILS
  - Microfluidic flow device assembly
  - Competition in liquid shaking culture
  - Biofilm culture conditions
  - Mathematical models
  - Biofilm invasion assay
  - Biofilm dispersal rate and colonization assay
  - Fluorescence microscopy
  - Image analysis
- QUANTIFICATION AND STATISTICAL ANALYSIS

SUPPLEMENTAL INFORMATION

Supplemental information can be found online at https://doi.org/10.1016/j.cub.2024.07.078.

ACKNOWLEDGMENTS

We thank members of the Nadell lab and the microbiology community at Dartmouth for their feedback on the project. C.D.N. received support from the Human Frontier Science Program (award number RGY0077/2020), the Simons Foundation (award number 826672), NSF IOS grant 2017879, and NIGMS grant 1R35GM151158-01.

AUTHOR CONTRIBUTIONS

J.D.H. and C.D.N. conceived the study and designed the models and experiments. J.D.H. performed all experiments, modeling, quantification, primary analysis, and figure generation. D.S. provided key support on completing the mean-field and reaction-diffusion models. J.D.H. and C.D.N. wrote the paper.

DECLARATION OF INTERESTS

The authors declare no competing interests.

Received: December 11, 2023
Revised: April 25, 2024
Accepted: July 22, 2024
Published: August 19, 2024

REFERENCES

1. Persat, A., Nadell, C.D., Kim, M.K., Ingremeau, F., Siryaporn, A., Drescher, K., Wingreen, N.S., Bassler, B.L., Gitai, Z., and Stone, H.A. (2015). The mechanical world of bacteria. Cell *161*, 988–997. https://doi.org/10.1016/j.cell.2015.05.005.
2. Chew, S.C., and Yang, L. (2017). Biofilms: microbial cities wherein flow shapes competition. Trends Microbiol. *25*, 331–332. https://doi.org/10.1016/j.tim.2017.02.007.
3. Ch'ng, J.-H., Chong, K.K.L., Lam, L.N., Wong, J.J., and Kline, K.A. (2019). Biofilm-associated infection by enterococci. Nat. Rev. Microbiol. *17*, 82–94. https://doi.org/10.1038/s41579-018-0107-z.
4. Ma, L.Z., Wang, D., Liu, Y., Zhang, Z., and Wozniak, D.J. (2022). Regulation of biofilm exopolysaccharide biosynthesis and degradation in *Pseudomonas aeruginosa*. Annu. Rev. Microbiol. *76*, 413–433. https://doi.org/10.1146/annurev-micro-041320-111355.
5. Serra, D.O., and Hengge, R. (2021). Bacterial multicellularity: the biology of *Escherichia coli* building large-scale biofilm communities. Annu. Rev. Microbiol. *75*, 269–290. https://doi.org/10.1146/annurev-micro-031921-055801.
6. Teschler, J.K., Nadell, C.D., Drescher, K., and Yildiz, F.H. (2022). Mechanisms underlying *Vibrio cholerae* biofilm formation and dispersion. Annu. Rev. Microbiol. *76*, 503–532. https://doi.org/10.1146/annurev-micro-111021-053553.
7. Flemming, H.-C., Van Hullebusch, E.D., Neu, T.R., Nielsen, P.H., Seviour, T., Stoodley, P., Wingender, J., and Wuertz, S. (2023). The biofilm matrix: multitasking in a shared space. Nat. Rev. Microbiol. *21*, 70–86. https://doi.org/10.1038/s41579-022-00791-0.
8. Sauer, K., Stoodley, P., Goeres, D.M., Hall-Stoodley, L., Burmølle, M., Stewart, P.S., and Bjarnsholt, T. (2022). The biofilm life cycle: expanding the conceptual model of biofilm formation. Nat. Rev. Microbiol. *20*, 608–620. https://doi.org/10.1038/s41579-022-00767-0.
9. Donlan, R.M. (2002). Biofilms: microbial life on surfaces. Emerg. Infect. Dis. *8*, 881–890. https://doi.org/10.3201/eid0809.020063.
10. Hibbing, M.E., Fuqua, C., Parsek, M.R., and Peterson, S.B. (2010). Bacterial competition: surviving and thriving in the microbial jungle. Nat. Rev. Microbiol. *8*, 15–25. https://doi.org/10.1038/nrmicro2259.
11. Nadell, C.D., Xavier, J.B., and Foster, K.R. (2009). The sociobiology of biofilms. FEMS Microbiol. Rev. *33*, 206–224. https://doi.org/10.1111/j.1574-6976.2008.00150.x.
12. Granato, E.T., Meiller-Legrand, T.A., and Foster, K.R. (2019). The evolution and ecology of bacterial warfare. Curr. Biol. *29*, R521–R537. https://doi.org/10.1016/j.cub.2019.04.024.

13. Foster, K.R., and Bell, T. (2012). Competition, not cooperation, dominates interactions among culturable microbial species. Curr. Biol. *22*, 1845–1850. https://doi.org/10.1016/j.cub.2012.08.005.

14. Rendueles, O., and Ghigo, J.-M. (2015). Mechanisms of competition in biofilm communities. Microbiol. Spectr. *3*, 3.3.28. https://doi.org/10.1128/microbiolspec.MB-0009-2014.

15. Xavier, J.B., and Foster, K.R. (2007). Cooperation and conflict in microbial biofilms. Proc. Natl. Acad. Sci. USA *104*, 876–881. https://doi.org/10.1073/pnas.0607651104.

16. Nadell, C.D., Drescher, K., and Foster, K.R. (2016). Spatial structure, cooperation and competition in biofilms. Nat. Rev. Microbiol. *14*, 589–600. https://doi.org/10.1038/nrmicro.2016.84.

17. Palmer, J.D., and Foster, K.R. (2022). Bacterial species rarely work together. Science *376*, 581–582. https://doi.org/10.1126/science.abn5093.

18. Oliveira, N.M., Niehus, R., and Foster, K.R. (2014). Evolutionary limits to cooperation in microbial communities. Proc. Natl. Acad. Sci. USA *111*, 17941–17946. https://doi.org/10.1073/pnas.1412673111.

19. Levin, S.A. (1970). Community equilibria and stability, and an extension of the competitive exclusion principle. Am. Nat. *104*, 413–423. https://doi.org/10.1086/282676.

20. Ellner, S.P., Snyder, R.E., Adler, P.B., and Hooker, G. (2022). Toward a "modern coexistence theory" for the discrete and spatial. Ecol. Monogr. *92*, e1548. https://doi.org/10.1002/ecm.1548.

21. Ellner, S.P., Snyder, R.E., Adler, P.B., and Hooker, G. (2019). An expanded modern coexistence theory for empirical applications. Ecol. Lett. *22*, 3–18. https://doi.org/10.1111/ele.13159.

22. Barabás, G., D'Andrea, R., and Stump, S.M. (2018). Chesson's coexistence theory. Ecol. Monogr. *88*, 277–303. https://doi.org/10.1002/ecm.1302.

23. HilleRisLambers, J., Adler, P.B., Harpole, W.S., Levine, J.M., and Mayfield, M.M. (2012). Rethinking community assembly through the lens of coexistence theory. Annu. Rev. Ecol. Evol. Syst. *43*, 227–248. https://doi.org/10.1146/annurev-ecolsys-110411-160411.

24. Chesson, P. (2000). General theory of competitive coexistence in spatially-varying environments. Theor. Popul. Biol. *58*, 211–237. https://doi.org/10.1006/tpbi.2000.1486.

25. McPeek, M.A. (2022). Coexistence in Ecology: A Mechanistic Perspective (Princeton University Press).

26. Chesson, P. (2000). Mechanisms of maintenance of species diversity. Annu. Rev. Ecol. Syst. *31*, 343–366. https://doi.org/10.1146/annurev.ecolsys.31.1.343.

27. McDougald, D., Rice, S.A., Barraud, N., Steinberg, P.D., and Kjelleberg, S. (2011). Should we stay or should we go: mechanisms and ecological consequences for biofilm dispersal. Nat. Rev. Microbiol. *10*, 39–50. https://doi.org/10.1038/nrmicro2695.

28. Monds, R.D., and O'Toole, G.A. (2009). The developmental model of microbial biofilms: ten years of a paradigm up for review. Trends Microbiol. *17*, 73–87. https://doi.org/10.1016/j.tim.2008.11.001.

29. Jo, J., Price-Whelan, A., and Dietrich, L.E.P. (2022). Gradients and consequences of heterogeneity in biofilms. Nat. Rev. Microbiol. *20*, 593–607. https://doi.org/10.1038/s41579-022-00692-2.

30. Stewart, P.S., and Franklin, M.J. (2008). Physiological heterogeneity in biofilms. Nat. Rev. Microbiol. *6*, 199–210. https://doi.org/10.1038/nrmicro1838.

31. Wimpenny, J., Manz, W., and Szewzyk, U. (2000). Heterogeneity in biofilms. FEMS Microbiol. Rev. *24*, 661–671. https://doi.org/10.1111/j.1574-6976.2000.tb00565.x.

32. Katharios-Lanwermeyer, S., and O'Toole, G.A. (2022). Biofilm maintenance as an active process: evidence that biofilms work hard to stay put. J. Bacteriol. *204*, e0058721. https://doi.org/10.1128/jb.00587-21.

33. Chave, J. (2013). The problem of pattern and scale in ecology: what have we learned in 20 years? Ecol. Lett. *16*, 4–16. https://doi.org/10.1111/ele.12048.

34. Levin, S.A. (1992). The problem of pattern and scale in ecology: the Robert H. MacArthur award lecture. Ecology *73*, 1943–1967. https://doi.org/10.2307/1941447.

35. Oumer, Y., Regasa Dadi, B., Seid, M., Biresaw, G., and Manilal, A. (2021). Catheter-associated urinary tract infection: incidence, associated factors and drug resistance patterns of bacterial isolates in Southern Ethiopia. Infect. Drug Resist. *14*, 2883–2894. https://doi.org/10.2147/IDR.S311229.

36. Nicolle, L.E. (2014). Catheter associated urinary tract infections. Antimicrob. Resist. Infect. Control *3*, 23. https://doi.org/10.1186/2047-2994-3-23.

37. M.A. Mulvey, D.J. Klumpp, and A.E. Stapleton, eds. (2017). Urinary Tract Infections: Molecular Pathogenesis and Clinical Management, Second Edition (ASM Press).

38. Laganenka, L., and Sourjik, V. (2018). Autoinducer 2-dependent Escherichia coli biofilm formation is enhanced in a dual-species coculture. Appl. Environ. Microbiol. *84*, e02638. https://doi.org/10.1128/AEM.02638-17.

39. Chia, T.W.R., Nguyen, V.T., McMeekin, T., Fegan, N., and Dykes, G.A. (2011). Stochasticity of bacterial attachment and its predictability by the extended Derjaguin-Landau-Verwey-Overbeek theory. Appl. Environ. Microbiol. *77*, 3757–3764. https://doi.org/10.1128/AEM.01415-10.

40. Lee, C.K., Vachier, J., de Anda, J., Zhao, K., Baker, A.E., Bennett, R.R., Armbruster, C.R., Lewis, K.A., Tarnopol, R.L., Lomba, C.J., et al. (2020). Social cooperativity of bacteria during reversible surface attachment in young biofilms: a quantitative comparison of *Pseudomonas aeruginosa* PA14 and PAO1. mBio *11*, e02644. https://doi.org/10.1128/mBio.02644-19.

41. Sanchez, A., and Golding, I. (2013). Genetic determinants and cellular constraints in noisy gene expression. Science *342*, 1188–1193. https://doi.org/10.1126/science.1242975.

42. Harmsen, M., Yang, L., Pamp, S.J., and Tolker-Nielsen, T. (2010). An update on *Pseudomonas aeruginosa* biofilm formation, tolerance, and dispersal. FEMS Immunol. Med. Microbiol. *59*, 253–268. https://doi.org/10.1111/j.1574-695X.2010.00690.x.

43. Klausen, M., Gjermansen, M., Kreft, J.-U., and Tolker-Nielsen, T. (2006). Dynamics of development and dispersal in sessile microbial communities: examples from *Pseudomonas aeruginosa* and *Pseudomonas putida* model biofilms. FEMS Microbiol. Lett. *261*, 1–11. https://doi.org/10.1111/j.1574-6968.2006.00280.x.

44. Taylor, T.B., and Buckling, A. (2010). Competition and dispersal in *Pseudomonas aeruginosa*. Am. Nat. *176*, 83–89. https://doi.org/10.1086/652995.

45. Purevdorj-Gage, B., Costerton, W.J., and Stoodley, P. (2005). Phenotypic differentiation and seeding dispersal in non-mucoid and mucoid Pseudomonas aeruginosa biofilms. Microbiology (Reading) *151*, 1569–1576. https://doi.org/10.1099/mic.0.27536-0.

46. Rasamiravaka, T., Labtani, Q., Duez, P., and El Jaziri, M. (2015). The formation of biofilms by *Pseudomonas aeruginosa*: a review of the natural and synthetic compounds interfering with control mechanisms. BioMed Res. Int. *2015*, 759348. https://doi.org/10.1155/2015/759348.

47. Dong, Y.-H., Zhang, X.-F., An, S.-W., Xu, J.-L., and Zhang, L.-H. (2008). A novel two-component system BqsS-BqsR modulates quorum sensing-dependent biofilm decay in *Pseudomonas aeruginosa*. Commun. Integr. Biol. *1*, 88–96. https://doi.org/10.4161/cib.1.1.6717.

48. Reis, R.S., Pereira, A.G., Neves, B.C., and Freire, D.M.G. (2011). Gene regulation of rhamnolipid production in Pseudomonas aeruginosa – a review. Bioresour. Technol. *102*, 6377–6384. https://doi.org/10.1016/j.biortech.2011.03.074.

49. Boles, B.R., Thoendel, M., and Singh, P.K. (2005). Rhamnolipids mediate detachment of *Pseudomonas aeruginosa* from biofilms. Mol. Microbiol. *57*, 1210–1223. https://doi.org/10.1111/j.1365-2958.2005.04743.x.

50. Schooling, S.R., Charaf, U.K., Allison, D.G., and Gilbert, P. (2004). A role for rhamnolipid in biofilm dispersion. Biofilms *1*, 91–99. https://doi.org/10.1017/S147905050400119X.

51. Davey, M.E., Caiazza, N.C., and O'Toole, G.A. (2003). Rhamnolipid surfactant production affects biofilm architecture in *Pseudomonas aeruginosa* PAO1. J. Bacteriol. *185*, 1027–1036. https://doi.org/10.1128/JB.185.3.1027-1036.2003.

52. McPeek, M.A. (2012). Intraspecific density dependence and a guild of consumers coexisting on one resource. Ecology *93*, 2728–2735. https://doi.org/10.1890/12-0797.1.

53. McPeek, M.A. (2019). Mechanisms influencing the coexistence of multiple consumers and multiple resources: resource and apparent competition. Ecol. Monogr. *89*, e01328. https://doi.org/10.1002/ecm.1328.

54. Barabás, G., J Michalska-Smith, M., and Allesina, S. (2016). The effect of intra- and interspecific competition on coexistence in multispecies communities. Am. Nat. *188*, E1–E12. https://doi.org/10.1086/686901.

55. Du, X., Zhou, S., and Etienne, R.S. (2011). Negative density dependence can offset the effect of species competitive asymmetry: A niche-based mechanism for neutral-like patterns. J. Theor. Biol. *278*, 127–134. https://doi.org/10.1016/j.jtbi.2011.03.003.

56. Kaplan, J.B. (2010). Biofilm dispersal: mechanisms, clinical implications, and potential therapeutic uses. J. Dent. Res. *89*, 205–218. https://doi.org/10.1177/0022034509359403.

57. Rumbaugh, K.P., and Sauer, K. (2020). Biofilm dispersion. Nat. Rev. Microbiol. *18*, 571–586. https://doi.org/10.1038/s41579-020-0385-0.

58. Sauer, K., Cullen, M.C., Rickard, A.H., Zeef, L.A.H., Davies, D.G., and Gilbert, P. (2004). Characterization of nutrient-induced dispersion in *Pseudomonas aeruginosa* PAO1 biofilm. J. Bacteriol. *186*, 7312–7326. https://doi.org/10.1128/JB.186.21.7312-7326.2004.

59. Wood, T.L., Gong, T., Zhu, L., Miller, J., Miller, D.S., Yin, B., and Wood, T.K. (2018). Rhamnolipids from Pseudomonas aeruginosa disperse the biofilms of sulfate-reducing bacteria. npj Biofilms Microbiomes *4*, 22. https://doi.org/10.1038/s41522-018-0066-1.

60. Irie, Y., O'Toole, G.A., and Yuk, M.H. (2005). *Pseudomonas aeruginosa* rhamnolipids disperse *Bordetella bronchiseptica* biofilms. FEMS Microbiol. Lett. *250*, 237–243. https://doi.org/10.1016/j.femsle.2005.07.012.

61. Levins, R., and Culver, D. (1971). Regional coexistence of species and competition between rare species. Proc. Natl. Acad. Sci. USA *68*, 1246–1248. https://doi.org/10.1073/pnas.68.6.1246.

62. Yu, D.W., and Wilson, H.B. (2001). The competition-colonization trade-off is dead; long live the competition-colonization trade-off. Am. Nat. *158*, 49–63. https://doi.org/10.1086/320865.

63. Wetherington, M.T., Nagy, K., Dér, L., Ábrahám, Á., Noorlag, J., Galajda, P., and Keymer, J.E. (2022). Ecological succession and the competition-colonization trade-off in microbial communities. BMC Biol. *20*, 262. https://doi.org/10.1186/s12915-022-01462-5.

64. Hastings, A. (1980). Disturbance, coexistence, history, and competition for space. Theor. Popul. Biol. *18*, 363–373. https://doi.org/10.1016/0040-5809(80)90059-3.

65. Turnbull, L.A., Coomes, D., Hector, A., and Rees, M. (2004). Seed mass and the competition/colonization trade-off: competitive interactions and spatial patterns in a guild of annual plants. J. Ecol. *92*, 97–109. https://doi.org/10.1111/j.1365-2745.2004.00856.x.

66. Nadell, C.D., and Bassler, B.L. (2011). A fitness trade-off between local competition and dispersal in *Vibrio cholerae* biofilms. Proc. Natl. Acad. Sci. USA *108*, 14181–14185. https://doi.org/10.1073/pnas.1111147108.

67. Gude, S., Pinçe, E., Taute, K.M., Seinen, A.-B., Shimizu, T.S., and Tans, S.J. (2020). Bacterial coexistence driven by motility and spatial competition. Nature *578*, 588–592. https://doi.org/10.1038/s41586-020-2033-2.

68. Amarasekare, P. (2004). Spatial variation and density-dependent dispersal in competitive coexistence. Proc. Biol. Sci. *271*, 1497–1506. https://doi.org/10.1098/rspb.2004.2696.

69. Kreamer, N.N.K., Wilks, J.C., Marlow, J.J., Coleman, M.L., and Newman, D.K. (2012). BqsR/BqsS constitute a two-component system that senses extracellular Fe(II) in Pseudomonas aeruginosa. J. Bacteriol. *194*, 1195–1204. https://doi.org/10.1128/JB.05634-11.

70. Sultan, M., Arya, R., and Kim, K.K. (2021). Roles of two-component systems in Pseudomonas aeruginosa virulence. Int. J. Mol. Sci. *22*, 12152. https://doi.org/10.3390/ijms222212152.

71. Wang, B.X., Cady, K.C., Oyarce, G.C., Ribbeck, K., and Laub, M.T. (2021). Two-component signaling systems regulate diverse virulence-associated traits in Pseudomonas aeruginosa. Appl. Environ. Microbiol. *87*, e03089. https://doi.org/10.1128/AEM.03089-20.

72. Grainger, T.N., Levine, J.M., and Gilbert, B. (2019). The invasion criterion: A common currency for ecological research. Trends Ecol. Evol. *34*, 925–935. https://doi.org/10.1016/j.tree.2019.05.007.

73. Levine, J.M., Bascompte, J., Adler, P.B., and Allesina, S. (2017). Beyond pairwise mechanisms of species coexistence in complex communities. Nature *546*, 56–64. https://doi.org/10.1038/nature22898.

74. Winans, J.B., Wucher, B.R., and Nadell, C.D. (2022). Multispecies biofilm architecture determines bacterial exposure to phages. PLoS Biol. *20*, e3001913. https://doi.org/10.1371/journal.pbio.3001913.

75. Vidakovic, L., Singh, P.K., Hartmann, R., Nadell, C.D., and Drescher, K. (2018). Dynamic biofilm architecture confers individual and collective mechanisms of viral protection. Nat. Microbiol. *3*, 26–31. https://doi.org/10.1038/s41564-017-0050-1.

76. Matz, C., McDougald, D., Moreno, A.M., Yung, P.Y., Yildiz, F.H., and Kjelleberg, S. (2005). Biofilm formation and phenotypic variation enhance predation-driven persistence of *Vibrio cholerae*. Proc. Natl. Acad. Sci. USA *102*, 16819–16824. https://doi.org/10.1073/pnas.0505350102.

77. Smith, W.P.J., Wucher, B.R., Nadell, C.D., and Foster, K.R. (2023). Bacterial defences: mechanisms, evolution and antimicrobial resistance. Nat. Rev. Microbiol. *21*, 519–534. https://doi.org/10.1038/s41579-023-00877-3.

78. Díaz-Pascual, F., Hartmann, R., Lempp, M., Vidakovic, L., Song, B., Jeckel, H., Thormann, K.M., Yildiz, F.H., Dunkel, J., Link, H., et al. (2019). Breakdown of Vibrio cholerae biofilm architecture induced by antibiotics disrupts community barrier function. Nat. Microbiol. *4*, 2136–2145. https://doi.org/10.1038/s41564-019-0579-2.

79. Wucher, B.R., Winans, J.B., Elsayed, M., Kadouri, D.E., and Nadell, C.D. (2023). Breakdown of clonal cooperative architecture in multispecies biofilms and the spatial ecology of predation. Proc. Natl. Acad. Sci. USA *120*, e2212650120. https://doi.org/10.1073/pnas.2212650120.

80. Goh, Y.F., Røder, H.L., Chan, S.H., Ismail, M.H., Madsen, J.S., Lee, K.W.K., Sørensen, S.J., Givskov, M., Burmølle, M., Rice, S.A., et al. (2023). Associational resistance to predation by protists in a mixed species biofilm. Appl. Environ. Microbiol. *89*, e0174122. https://doi.org/10.1128/aem.01741-22.

81. Stoodley, P., Sauer, K., Davies, D.G., and Costerton, J.W. (2002). Biofilms as complex differentiated communities. Annu. Rev. Microbiol. *56*, 187–209. https://doi.org/10.1146/annurev.micro.56.012302.160705.

82. Burmølle, M., Ren, D., Bjarnsholt, T., and Sørensen, S.J. (2014). Interactions in multispecies biofilms: do they actually matter? Trends Microbiol. *22*, 84–91. https://doi.org/10.1016/j.tim.2013.12.004.

83. Mitri, S., Xavier, J.B., and Foster, K.R. (2011). Social evolution in multispecies biofilms. Proc. Natl. Acad. Sci. USA *108*, 10839–10846. https://doi.org/10.1073/pnas.1100292108.

84. Rittman, B.E. (1982). The effect of shear stress on biofilm loss rate. Biotechnol. Bioeng. *24*, 501–506. https://doi.org/10.1002/bit.260240219.

85. Rice, S.A., Koh, K.S., Queck, S.Y., Labbate, M., Lam, K.W., and Kjelleberg, S. (2005). Biofilm formation and sloughing in *Serratia marcescens* are controlled by quorum sensing and nutrient cues. J. Bacteriol. *187*, 3477–3485. https://doi.org/10.1128/JB.187.10.3477-3485.2005.

86. Barraud, N., Hassett, D.J., Hwang, S.-H., Rice, S.A., Kjelleberg, S., and Webb, J.S. (2006). Involvement of nitric oxide in biofilm dispersal of

Pseudomonas aeruginosa. J. Bacteriol. *188*, 7344–7353. https://doi.org/10.1128/JB.00779-06.

87. Díaz-Salazar, C., Calero, P., Espinosa-Portero, R., Jiménez-Fernández, A., Wirebrand, L., Velasco-Domínguez, M.G., López-Sánchez, A., Shingler, V., and Govantes, F. (2017). The stringent response promotes biofilm dispersal in Pseudomonas putida. Sci. Rep. *7*, 18055. https://doi.org/10.1038/s41598-017-18518-0.
88. Nair, H.A.S., Subramoni, S., Poh, W.H., Hasnuddin, N.T.B., Tay, M., Givskov, M., Tolker-Nielsen, T., Kjelleberg, S., McDougald, D., and Rice, S.A. (2021). Carbon starvation of Pseudomonas aeruginosa biofilms selects for dispersal insensitive mutants. BMC Microbiol. *21*, 255. https://doi.org/10.1186/s12866-021-02318-8.
89. Battin, T.J., Besemer, K., Bengtsson, M.M., Romani, A.M., and Packmann, A.I. (2016). The ecology and biogeochemistry of stream biofilms. Nat. Rev. Microbiol. *14*, 251–263. https://doi.org/10.1038/nrmicro.2016.15.
90. Battin, T.J., Kaplan, L.A., Denis Newbold, J., and Hansen, C.M.E. (2003). Contributions of microbial biofilms to ecosystem processes in stream mesocosms. Nature *426*, 439–442. https://doi.org/10.1038/nature02152.
91. Rosentreter, J.A., Borges, A.V., Deemer, B.R., Holgerson, M.A., Liu, S., Song, C., Melack, J., Raymond, P.A., Duarte, C.M., Allen, G.H., et al. (2021). Half of global methane emissions come from highly variable aquatic ecosystem sources. Nat. Geosci. *14*, 225–230. https://doi.org/10.1038/s41561-021-00715-2.
92. Nadell, C.D., Ricaurte, D., Yan, J., Drescher, K., and Bassler, B.L. (2017). Flow environment and matrix structure interact to determine spatial competition in Pseudomonas aeruginosa biofilms. eLife *6*, e21855. https://doi.org/10.7554/eLife.21855.
93. Kasetty, S., Katharios-Lanwermeyer, S., O'Toole, G.A., and Nadell, C.D. (2021). Differential surface competition and biofilm invasion strategies of Pseudomonas aeruginosa PA14 and PAO1. J. Bacteriol. *203*, e0026521. https://doi.org/10.1128/JB.00265-21.
94. Jennings, L.K., Storek, K.M., Ledvina, H.E., Coulon, C., Marmont, L.S., Sadovskaya, I., Secor, P.R., Tseng, B.S., Scian, M., Filloux, A., et al. (2015). Pel is a cationic exopolysaccharide that cross-links extracellular DNA in the *Pseudomonas aeruginosa* biofilm matrix. Proc. Natl. Acad. Sci. USA *112*, 11353–11358. https://doi.org/10.1073/pnas.1503058112.
95. Colvin, K.M., Irie, Y., Tart, C.S., Urbano, R., Whitney, J.C., Ryder, C., Howell, P.L., Wozniak, D.J., and Parsek, M.R. (2012). The Pel and Psl polysaccharides provide Pseudomonas aeruginosa structural redundancy within the biofilm matrix. Environ. Microbiol. *14*, 1913–1928. https://doi.org/10.1111/j.1462-2920.2011.02657.x.
96. Lau, G.W., Hassett, D.J., Ran, H., and Kong, F. (2004). The role of pyocyanin in Pseudomonas aeruginosa infection. Trends Mol. Med. *10*, 599–606. https://doi.org/10.1016/j.molmed.2004.10.002.
97. Michel-Briand, Y., and Baysse, C. (2002). The pyocins of Pseudomonas aeruginosa. Biochimie *84*, 499–510. https://doi.org/10.1016/S0300-9084(02)01422-0.
98. Hassan, H.M., and Fridovich, I. (1980). Mechanism of the antibiotic action pyocyanine. J. Bacteriol. *141*, 156–163. https://doi.org/10.1128/jb.141.1.156-163.1980.
99. Wood, T.E., Howard, S.A., Förster, A., Nolan, L.M., Manoli, E., Bullen, N.P., Yau, H.C.L., Hachani, A., Hayward, R.D., Whitney, J.C., et al. (2019). The Pseudomonas aeruginosa T6SS delivers a periplasmic toxin that disrupts bacterial cell morphology. Cell Rep. *29*, 187–201.e7. https://doi.org/10.1016/j.celrep.2019.08.094.
100. Ghequire, M.G.K., and De Mot, R. (2014). Ribosomally encoded antibacterial proteins and peptides from *Pseudomonas*. FEMS Microbiol. Rev. *38*, 523–568. https://doi.org/10.1111/1574-6976.12079.
101. Recinos, D.A., Sekedat, M.D., Hernandez, A., Cohen, T.S., Sakhtah, H., Prince, A.S., Price-Whelan, A., and Dietrich, L.E.P. (2012). Redundant phenazine operons in *Pseudomonas aeruginosa* exhibit environment-dependent expression and differential roles in pathogenicity. Proc. Natl. Acad. Sci. USA *109*, 19420–19425. https://doi.org/10.1073/pnas.1213901109.
102. Tai, J.B., Mukherjee, S., Nero, T., Olson, R., Tithof, J., Nadell, C.D., and Yan, J. (2022). Social evolution of shared biofilm matrix components. Proc. Natl. Acad. Sci. USA *119*, e2123469119. https://doi.org/10.1073/pnas.2123469119.
103. Keogh, D., Tay, W.H., Ho, Y.Y., Dale, J.L., Chen, S., Umashankar, S., Williams, R.B.H., Chen, S.L., Dunny, G.M., and Kline, K.A. (2016). Enterococcal metabolite cues facilitate interspecies niche modulation and polymicrobial infection. Cell Host Microbe *20*, 493–503. https://doi.org/10.1016/j.chom.2016.09.004.
104. Reid, D.W., Anderson, G.J., and Lamont, I.L. (2009). Role of lung iron in determining the bacterial and host struggle in cystic fibrosis. Am. J. Physiol. Lung Cell. Mol. Physiol. *297*, L795–L802. https://doi.org/10.1152/ajplung.00132.2009.
105. Cox, C.D. (1986). Role of pyocyanin in the acquisition of iron from transferrin. Infect. Immun. *52*, 263–270. https://doi.org/10.1128/iai.52.1.263-270.1986.
106. de Lorenzo, V., and Timmis, K.N. (1994). Analysis and Construction of Stable Phenotypes in Gram-Negative Bacteria with Tn5- and Tn10-Derived Minitransposons (Academic Press).
107. Bond, M.C., Vidakovic, L., Singh, P.K., Drescher, K., and Nadell, C.D. (2021). Matrix-trapped viruses can prevent invasion of bacterial biofilms by colonizing cells. eLife *10*, e65355. https://doi.org/10.7554/eLife.65355.
108. Koeppen, K., Nymon, A., Barnaby, R., Bashor, L., Li, Z., Hampton, T.H., Liefeld, A.E., Kolling, F.W., LaCroix, I.S., Gerber, S.A., et al. (2021). Let-7b-5p in vesicles secreted by human airway cells reduces biofilm formation and increases antibiotic sensitivity of *P. aeruginosa*. Proc. Natl. Acad. Sci. USA *118*, e2105370118. https://doi.org/10.1073/pnas.2105370118.
109. The MathWorks Incorp. (2022). MATLAB Version: 9.13.0 (R2021a). https://www.mathworks.com.
110. Hartmann, R., Jeckel, H., Jelli, E., Singh, P.K., Vaidya, S., Bayer, M., Rode, D.K.H., Vidakovic, L., Díaz-Pascual, F., Fong, J.C.N., et al. (2021). Quantitative image analysis of microbial communities with BiofilmQ. Nat. Microbiol. *6*, 151–156. https://doi.org/10.1038/s41564-020-00817-4.
111. Pilgrim, M., and Willison, S. (2009). Dive Into Python 3 (Springer).
112. McKinney, W. (2010). Data structures for statistical computing in python. In Proceedings of the 9th Python in Science Conference, S. van der Walt, and J. Millman, eds., pp. 56–61. https://doi.org/10.25080/Majora-92bf1922-00a.
113. Hunter, J.D. (2007). Matplotlib: A 2D graphics environment. Comput. Sci. Eng. *9*, 90–95. https://doi.org/10.1109/MCSE.2007.55.
114. Waskom, M. (2021). seaborn: statistical data visualization. JOSS *6*, 3021. https://doi.org/10.21105/joss.03021.
115. SciPy 1.0 Contributors, Virtanen, P., Gommers, R., Oliphant, T.E., Haberland, M., Reddy, T., Cournapeau, D., Burovski, E., Peterson, P., Weckesser, W., et al. (2020). SciPy 1.0: fundamental algorithms for scientific computing in Python. Nat Methods *17*, 261–272. https://doi.org/10.1038/s41592-019-0686-2.
116. Pandas Development Team (2020). pandas-dev/pandas: Pandas. Zenodo. https://doi.org/10.5281/zenodo.3509134.
117. Harper, M. (2015). python-ternary: ternary Plots in Python. Zenodo. https://doi.org/10.5281/zenodo.594435.
118. van der Walt, S., Schönberger, J.L., Nunez-Iglesias, J., Boulogne, F., Warner, J.D., Yager, N., Gouillart, E., and Yu, T.; scikit-image contributors (2014). scikit-image: image processing in Python. PeerJ *2*, e453. https://doi.org/10.7717/peerj.453.
119. Schroth, M.N., Cho, J.J., Green, S.K., Kominos, S.D., and Microbiology Society Publishing. (2018). Epidemiology of Pseudomonas aeruginosa in agricultural areas. J. Med. Microbiol. *67*, 1191–1201. https://doi.org/10.1099/jmm.0.000758.
120. Mathee, K. (2018). Forensic investigation into the origin of Pseudomonas aeruginosa PA14 — old but not lost. J. Med. Microbiol. *67*, 1019–1021. https://doi.org/10.1099/jmm.0.000778.

121. Serra, D.O., Richter, A.M., and Hengge, R. (2013). Cellulose as an architectural element in spatially structured Escherichia coli biofilms. J. Bacteriol. *195*, 5540–5554. https://doi.org/10.1128/JB.00946-13.

122. Gold, O.G., Jordan, H.V., and Van Houte, J. (1975). The prevalence of enterococci in the human mouth and their pathogenicity in animal models. Arch. Oral Biol. *20*, 473–477. https://doi.org/10.1016/0003-9969(75)90236-8.

123. Otsu, N. (1979). A threshold selection method from gray-level histograms. IEEE Trans. Syst. Man Cybern. *9*, 62–66. https://doi.org/10.1109/TSMC.1979.4310076.

124. Harris, C.R., Millman, K.J., van der Walt, S.J., Gommers, R., Virtanen, P., Cournapeau, D., Wieser, E., Taylor, J., Berg, S., Smith, N.J., et al. (2020). Array programming with NumPy. Nature *585*, 357–362. https://doi.org/10.1038/s41586-020-2649-2.

Please cite this article in press as: Holt et al., Dispersal of a dominant competitor can drive multispecies coexistence in biofilms, Current Biology (2024), https://doi.org/10.1016/j.cub.2024.07.078

STAR★METHODS

KEY RESOURCES TABLE

REAGENT or RESOURCE	SOURCE	IDENTIFIER
Bacterial and virus strains		
E. coli, λ*pir*	de Lorenzo and Timmis[106]	S17-1
E. coli AR3110, KanR, mKate2	Bond et al.[107]	CNE761
E. coli AR3110, 6x-His *csgA*, KanR, mKate2	Bond et al.[107]	CNE775
E. faecalis, OG1RF, RifR, GFP	Gary Dunny's Lab	CNF9
P. aeruginosa PA14, GentR, mKo-k	Koeppen et al.[108]	CNP88
P. aeruginosa PA14, WT	Wang et al.[71]	CNP115
P. aeruginosa PA14, WT, GentR, mKo-k	This study	CNP117
P. aeruginosa PA14, WT, mKo-k	This study	CNP119
P. aeruginosa PA14, Δ*bqsS*,	Wang et al.[71]	CNP116
P. aeruginosa PA14, Δ*bqsS*, GentR, mKo-k	This study	CNP118
P. aeruginosa PA14, Δ*bqsS*, mKo-k	This study	CNP120
P. aeruginosa PA14, GentR, mKo-k	Koeppen et al.[108]	CNP88
Chemicals, peptides, and recombinant proteins		
Poly-dimethysiloxane (PDMS)	Dow Chemical Company SYLGARD 184	cat. #04019862
#1.5 glass coverslips	Azer Scientific	cat. #1152260
Inlet tubing	Cole Palmer	cat. #06417-11
27Gx1/2 needles	BD Precision	cat. #30510
1mL syringes	Brandzig	cat. #CMD2583
5mL syringes	Becton, Dickinson, and Company	cat. #00382903096466
Harvard Apparatus Pico Plus Elite syringe pumps	Harvard Apparatus	cat. #70-4506
Yeast extract	Sigma-Aldrich	cat. #70161
Agar powder	Thermo Scientific	cat. #A10752.36
Sodium chloride	Fisher Scientific	cat. #S271
Tryptone broth	Sigma-Aldrich	cat. #T7293
Sucrose	Sigma-Aldrich	cat. #S0389
Nalidixic acid	Sigma-Aldrich	cat. #N4382
Gentamycin	Sigma-Aldrich	cat. #G1264
Software and algorithms		
Zen Black	Zeiss	v14.0.0.0
Zen Blue	Zeiss	v3.4.91.00000
MATLAB	MathWorks[109]	vR2021a
BiofilmQ	Hartmann et al.[110]	v0.2.2
Paraview	Kitware	v9.4.1
Python	Python.org[111]	v3.8.8
Anaconda	Anaconda.org	v2021.05
Spyder	Spyder-ide.org	v4.2.5
NumPy	NumPy.org[112]	v1.20.1
Matplotlib	Matplotlib.org[113]	v3.3.4
seaborn	Seaborn.pydata.org[114]	v0.11.1
SciPy	Scipy.org[115]	v1.6.2
Pandas	Pandas.pydata.org[116]	v1.2.4
python-ternary	https://github.com/marcharper/python-ternary[117]	v1.0.8
palettable	https://github.com/jiffyclub/palettable	v3.3.3
scikit-image	Scikit-image.org[118]	v0.20.0

Please cite this article in press as: Holt et al., Dispersal of a dominant competitor can drive multispecies coexistence in biofilms, Current Biology (2024), https://doi.org/10.1016/j.cub.2024.07.078

RESOURCE AVAILABILITY

Lead contact

Further information and requests for resources and reagents should be directed to and will be fulfilled by the lead contact, Carey Nadell (carey.d.nadell@dartmouth.edu).

Materials availability

This study did not generate any new reagents.

Data and code availability

- Microscopy data reported in this paper will be shared by the lead contact upon request. The raw data used to generate plots is included in this paper's supplemental information.
- All code used to generate plots is accessible through: https://github.com/nadellinsilico/Disperse_Coexist_2023.
- Any additional information required to reanalyze the data reported in this paper is available from the lead contact upon request.

EXPERIMENTAL MODEL AND STUDY PARTICIPANT DETAILS

The *P. aeruginosa* strains used in this study were derived from PA14.[119,120] The *E. coli* strains were derived from AR3110, which is a modified K-12 W3110 strain with its natural extracellular matrix production restored.[121] The fluorescent *E. faecalis* strain OG1RF and was a gift of the Dunny laboratory.[122] The fluorescent protein expression construct insertions and the deletion mutants were made here and previously using standard allelic exchange. Gentamicin 60 μg/mL and nalidixic acid 50 μg/mL were used to select for *P. aeruginosa* after mating with *E. coli*. 10% sucrose *sacB* counter selection was then used to select for cells which had looped out the *sacB* portion of the plasmid. Cultures were grown overnight in lysogeny broth (LB, 10 g/L sodium chloride, 10 g/L tryptone, and 5 g/L yeast extract). Biofilm and planktonic cultures were grown in 1% tryptone broth.

METHOD DETAILS

Microfluidic flow device assembly

Microfluidic chambers for biofilm culture were made with polydimethylsiloxane (PDMS) using standard soft lithography techniques. PDMS was mixed and then cured on molds of chamber sets produced using photolithography, hole-punched for inlets and outlets, and bound to #1.5 36 mm by 60 mm glass coverslips via plasma cleaning. Constant flow was generated via Harvard Apparatus Pico Plus syringe pumps loaded with either 1 mL Brandzig plastic syringes or 5 mL BD syringes. Syringes had 25-gauge needles affixed to them that were fitted with #30 Cole Parmer PTFE tubing with an inner diameter of 0.3 mm. Inlet tubing for each chamber was affixed to the media syringe, and outlet tubing was run into a petri plate for waste collection or dispersal measurements (see below).

Competition in liquid shaking culture

Strains were grown overnight in LB medium at 37 degrees Celsius, with *P. aeruginosa* and *E. coli* being shaken at 250 rpm and *E. faecalis* being unshaken. All strains were then diluted to an OD_{600} of 0.2 in 1 % tryptone before being mixed at a 1:1:1 ratio. A 50 μL aliquot of this mixture was then transferred into 5 mL of 1% tryptone broth in a 15 mm culture tube with 2 glass beads to breakup aggregate formation. These cultures were shaken at 300 rpm. Every 24 h 50 μL was transferred into a fresh 5 mL of media. Relative abundance was measured every 24 h, immediately prior to dilution, by spotting 5 μL onto a glass coverslip and imaging 3 separate 212x212 μm fields of view.

Biofilm culture conditions

Strains were grown overnight in LB medium at 37 degrees Celsius, with *P. aeruginosa* and *E. coli* being shaken at 250 rpm and *E. faecalis* being unshaken. Overnight cultures were diluted to an OD_{600} of 0.2 in 1% tryptone before being mixed at a 1:1 ratio. The inoculum was then transferred into planar microfluidic devices measuring 5000 μm in length, 500 μm in width and 70 μm in height. After 1 h of incubation, 1% tryptone broth was introduced to the chamber at a rate of 0.05 μl/min (corresponding to an average flow velocity of 23.4 μm/s) at 22 degrees Celsius. To measure biomass within the chamber, the biofilm was imaged by confocal microscopy at z-intervals of 0.44 μm across 3 separate 212x212 μm fields of view. The BiofilmQ image processing framework was then used to perform image segmentation and quantification, and Python was used to perform statistical analysis and to produce figures.

Mathematical models

Our models build from the classical Lotka-Volterra model of interspecific competition:

$$\frac{dN_i}{dt} = r_i N_i \left(\frac{K_i - N_i - \Sigma(a_{ij} N_j)}{K_i} \right)$$

Please cite this article in press as: Holt et al., Dispersal of a dominant competitor can drive multispecies coexistence in biofilms, Current Biology (2024), https://doi.org/10.1016/j.cub.2024.07.078

where N_i is the mass of species i, r_i is the maximal growth rate of species i, K_i is the carrying capacity of species i, $a_{i,j}$ is the interaction coefficient between species i and j. To consider competition for a single resource within a fixed space, we define a_{ij} as r_i/r_j and we scale the carrying capacity to 1, giving:

$$\frac{dN_i}{dt} = r_i N_i \left(\frac{1 - N_i - \Sigma((r_j/r_i)N_j)}{K_i} \right)$$

Additionally, we add a dilution term, δ_i, to account for dispersal or removal from the system arriving at:

$$\frac{dN_i}{dt} = r_i N_i \left(\frac{1 - N_i - \Sigma((r_j/r_i)N_j)}{K_i} \right) - \delta_i N_i$$

The coupling of the equations implements direct competition for resources, with the abundance of one species being limited by the abundance of the other. The coefficients for such competitive interactions are given by the relative growth between the species r_j / r_i, which favor species that grow faster. Dispersal is triggered when the *P. aeruginosa* population reaches an upper threshold N_{up} and is implemented by a dispersal rate δ_i. Conversely, dispersal ceases when the *P. aeruginosa* population reaches a lower threshold N_{down}, restoring $\delta_i = 0$. We simulate this system using MATLAB ODE solver *ode113* to integrate the system of equations over time. We simulate the system piecewise, changing the parameter δ_i whenever the *P. aeruginosa* population crosses the upper or lower thresholds.

We model movement of the different species across a 2D surface by adding a diffusion term, arriving at a reaction-diffusion model consisting of a system of partial differential equations:

$$\partial N_i(\boldsymbol{x}, t)/\partial t = r_i N_i \left(1 - \frac{\sum_j (r_j/r_i) N_j}{K_i} \right) - \delta_i N_i + \mathrm{D_i} \nabla^2 N_i$$

Dispersal is triggered locally when the total *P. aeruginosa* population reaches the upper threshold N_{up}. We then simulate the model for an initial condition where the genotypes are randomly scattered across the surface. We use the Crank–Nicolson method, choosing time steps Δt and distance increments h such that $\Delta t < 0.5\ \Delta h^2 / D$ to guarantee the stability of the solution.

In our lattice-based model of interspecific competition, space is represented as a 2-dimensional discrete lattice sized 250x250 with periodic boundary conditions (the surface is a taurus). Each site can be vacant (state = 0) or occupied by a species of i (state=1,2,3). Individuals of type i are removed with probability S_i and give birth with probability β_i, and these probabilities are functions of the local environment. A type i born will try to occupy one of eight sites surrounding the seeding individual. If the chosen site is vacant, it changes to state i, otherwise nothing happens. When the simulation is run, at each time-step, sites are chosen at random to either replicate or become vacant. Movement to unoccupied grid sites is uniform for all three types.

The birth probability is set by the maximal growth rate for each species times the number of empty sites adjacent to each individual. The removal probability is set by the carrying capacity of each species times the number of occupied sites around each individual, rescaled to be the same order of magnitude as the maximal growth rate. This yields a single species stochastic-spatial model that is analogous to the ODE model:

$$\frac{dN_i}{dt} = r_i N_i \left(\frac{1 - N_i}{K_i} \right)$$

Since space is limited in the simulation to 250x250 grid nodes, competition occurs through the preferential occupation of free sites. For example, when a type dies it leaves a site open and whichever type can occupy that open site first will increase in abundance while the other type decreases in abundance. Increasing the maximal growth rate r gives an advantage in colonizing new sites while the population density is low. Increasing K gives an advantage in occupying vacant sites when the population density is high.

Mass dispersal events are implemented in a manner that matches our experimental data. At N_{up} dispersal occurs as an increase in *P. aeruginosa* death probability, and *P. aeruginosa* sites rapidly become unoccupied. At N_{down} dispersal stops and the death probability returns to normal. For all figures, we ran simulations with the same random seed. The MATLAB and Python scripts used to generate model figures are publicly available on GitHub and Zenodo. Parameters can be found in the Table S1.

Biofilm invasion assay

Cultures were grown for 4 d as described above. After 4 d of growth, the influx syringe was swapped to a new one containing one species resuspended in fresh media for 2 h. To prepare the invading strain, overnight cultures were back diluted into 50 mL of 1% tryptone and grown until mid-exponential phase. The mid-exponential phase cultures were then concentrated to an OD_{600} of 6.0. The media influent was swapped back to sterile 1% tryptone after 1 h of flow of the invading species at 0.05 μl/min. Imaging was then done at time 2 h and time 18 h post invasion. The growth of the invading strains was calculated by subtracting the invading species biovolume at 18 h from that at 2 h. The biovolume of strains was measured by imaging z-stacks of three separate 212x212 μm locations within each replicate chamber.

Please cite this article in press as: Holt et al., Dispersal of a dominant competitor can drive multispecies coexistence in biofilms, Current Biology (2024), https://doi.org/10.1016/j.cub.2024.07.078

Biofilm dispersal rate and colonization assay

Cultures were grown for 12 d as previously described in the biofilm culture conditions. After 12 d of growth, each biofilm was imaged, and the effluent tube was cut to 2 cm and attached to a fresh microfluidic chip to allow for colonization of a new surface. To measure the dispersal rate, the effluent tube was put into a 1.5 mL centrifuge tube with parafilm wax affixed over the top to allow for collection, while avoiding both contamination and desiccation. These samples were serially diluted, inoculated onto agar plates, and single colony forming units were distinguished by their morphology and fluorescent marker. For the colonization assay, flow into the fresh chamber ran for 2 h. For the dispersal assay, flow into the collection tube ran for 1 h to minimize growth of planktonic cells in the collected media prior to plating for CFUs. To measure the volume of colonizing cells, z-stacks of three separate 212x212 μm fields of view were acquired in the naïve chip immediately after the 2 h period of flow.

Fluorescence microscopy

All fluorescence imaging was performed using a Zeiss 880 line-scanning confocal microscope, using a 40x/1.2 N.A. water objective. The GFP protein expressed constitutively by *E. faecalis* was excited with a 488-laser line. The mKO-κ protein that P. aeruginosa expresses constitutively was excited with a 543-laser line. The mKate2 protein that *E. coli* expresses constitutively was excited with a 594-laser line. All representative images were processed by constrained iterative deconvolution in ZEN blue.

Image analysis

Native Zeiss CZI files produced by ZEN software were converted to.tiff stacks prior to being loaded into BiofilmQ, which was run using Matlab.[109] Biovolume thresholding was performed using either Otsu's method or Robust Background with a manual sensitivity adjustment.[110,123] The segmented biovolumes for all three species were cross-checked for thresholding accuracy against the raw image data, and then dissected into a 3-D grid with cube side lengths set to 2.3 μm (giving cubes that can maximally hold ~10 cells). The cube compartments were then used for all subsequent spatially resolved analysis. Calculated parameters were exported from BiofilmQ as.mat files and loaded into Python, where SciPy, seaborn, Pandas, NumPy, and Matplotlib were used for running statistical tests and figure generation.[111–116,118,124] For calculated cube-based parameters that require a range, we chose 10 μm as the range over which to measure (see main text for additional explanation). Operation of BiofilmQ and its array of analytical methods is described in extensive detail in Hartmann et al.[110]

QUANTIFICATION AND STATISTICAL ANALYSIS

At least three biological replicates, each defined as a single microcosm (microfluidic chamber or culture tube), were performed for each experiment across multiple weeks. For biofilm biovolume measurements, 3 regions of 212x212 μm were sampled as technical replicates within a chamber and averaged for each biological replicate. For liquid shaking culture relative abundance measurements, cells were placed between a cover slip and 3 regions of 212x212 μm were sampled and averaged for each biological replicate.

Seaborne v0.11.1 was used to generate linear regression plots. For all linear regression plots, the shaded area is the 95% confidence interval. For time resolved biofilm data, the shaded area is one standard deviation above and below the mean. Error bars denote the standard error of the mean. For box and whisker plots, the orange bar denotes the median, the box bounds denote first and third quartiles, and the whiskers denote the first and third quartiles plus 1.5 times the interquartile range. Ternary plots were either generated in python using the python-ternary library or in MATLAB using a custom script.[117] For all BiofilmQ-generated, cube-based data, mean values are weighted by biovolume for each species to account for cubes containing differing proportions of the total population. The Python scripts and corresponding datasheets used to generate figures and reported statistics are publicly available on GitHub and Zenodo.

Current Biology, Volume *34*

Supplemental Information

Dispersal of a dominant competitor can drive multispecies coexistence in biofilms

Jacob D. Holt, Daniel Schultz, and Carey D. Nadell

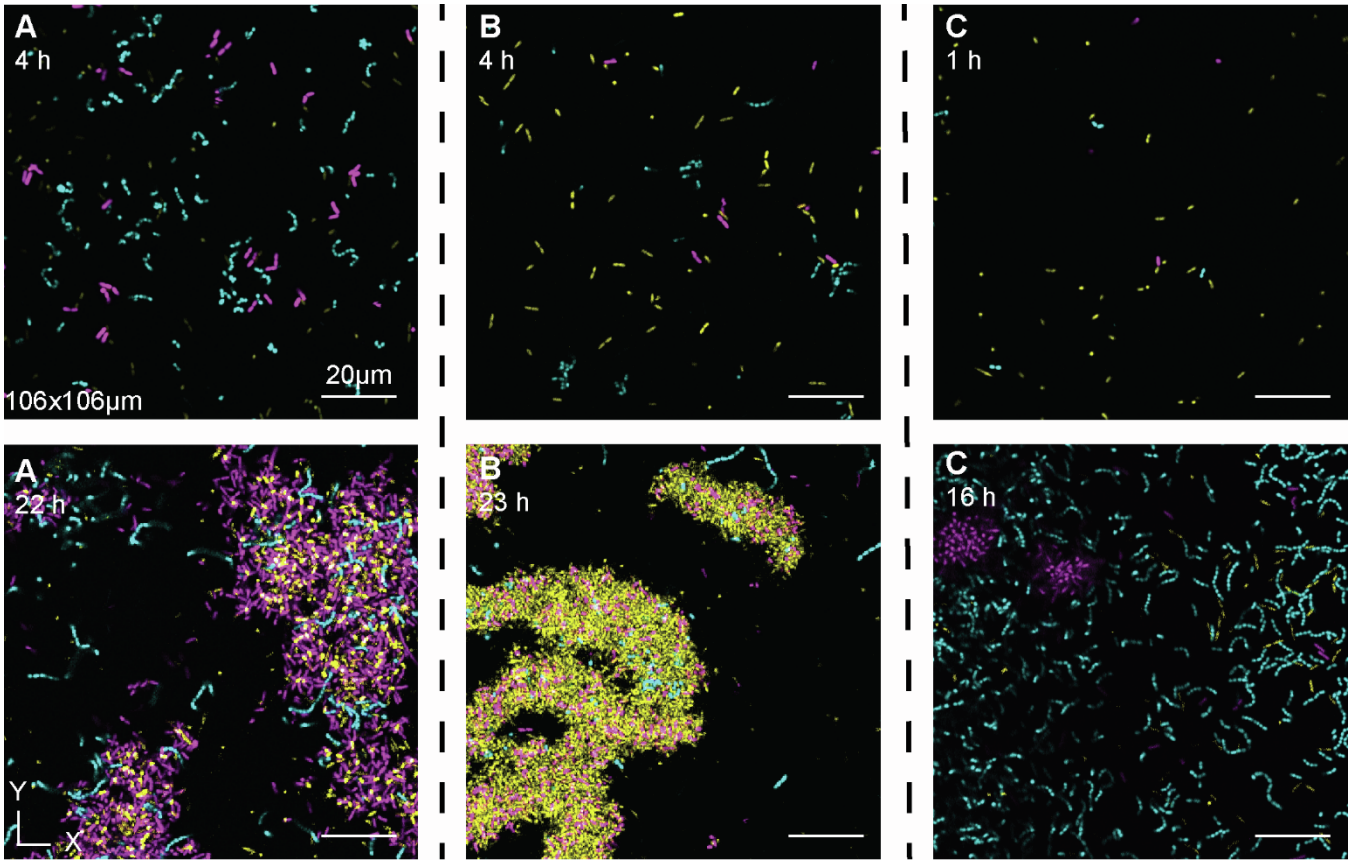

Figure S1. Representative images of variation in initial timepoints from three independent biofilm replicates, related to Figure 1.

(A) Shows an *E. coli* dominated early time point. **(B)** Shows a *P. aeruginosa* dominated initial timepoint. **(C)** Shows an *E. faecalis* dominated early time point. *P. aeruginosa* is shown in yellow, *E. coli* is shown in purple, and *E. faecalis* is shown in cyan.

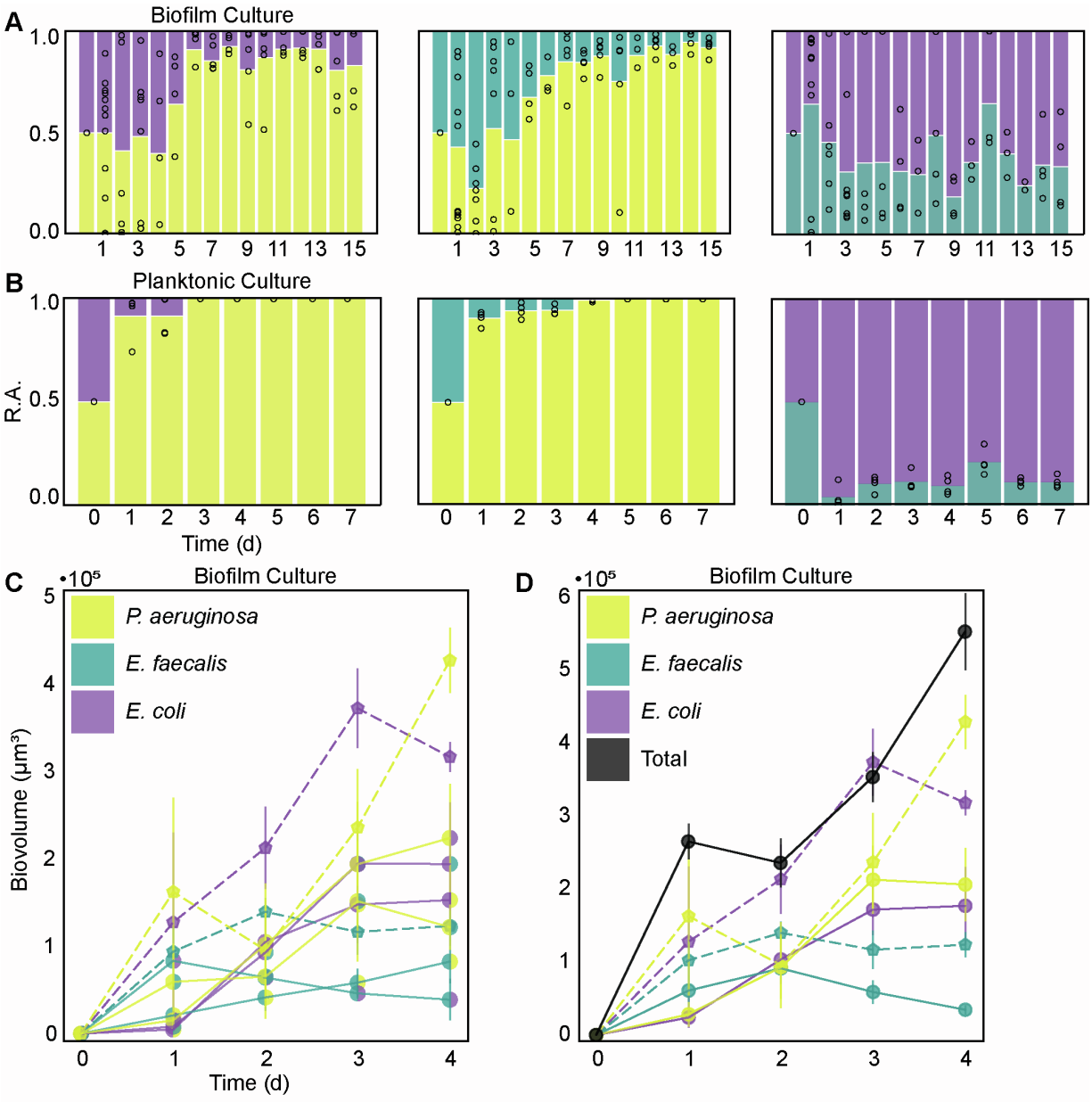

Figure S2. Competition in pairwise biofilm cocultures, related to Figure 1.
(A) Pairwise biofilm co-cultures of species relative abundance plotted against time (n=3-10). **(B)** Pairwise planktonic co-cultures of species relative abundance plotted against time (n=3-4). **(C)** The biovolume for each species in co-culture (solid lines) plotted alongside monoculture biofilm control experiments (dashed lines) for each species across the first four days of growth (n=3-8). **(D)** The biovolume of each species in tri-culture (solid lines) plotted alongside monoculture biofilm control experiments (dashed lines) for each species across the first four days of growth. Dots represent the mean and error bars represent standard error. The color of the line represents the strain being plotted and the color of the dots represents the strains present in the culture. *P. aeruginosa* is shown in yellow, *E. coli* is shown in purple, and *E. faecalis* is shown in cyan. The sum of the three species biovolume when grown together as a community is shown in black.

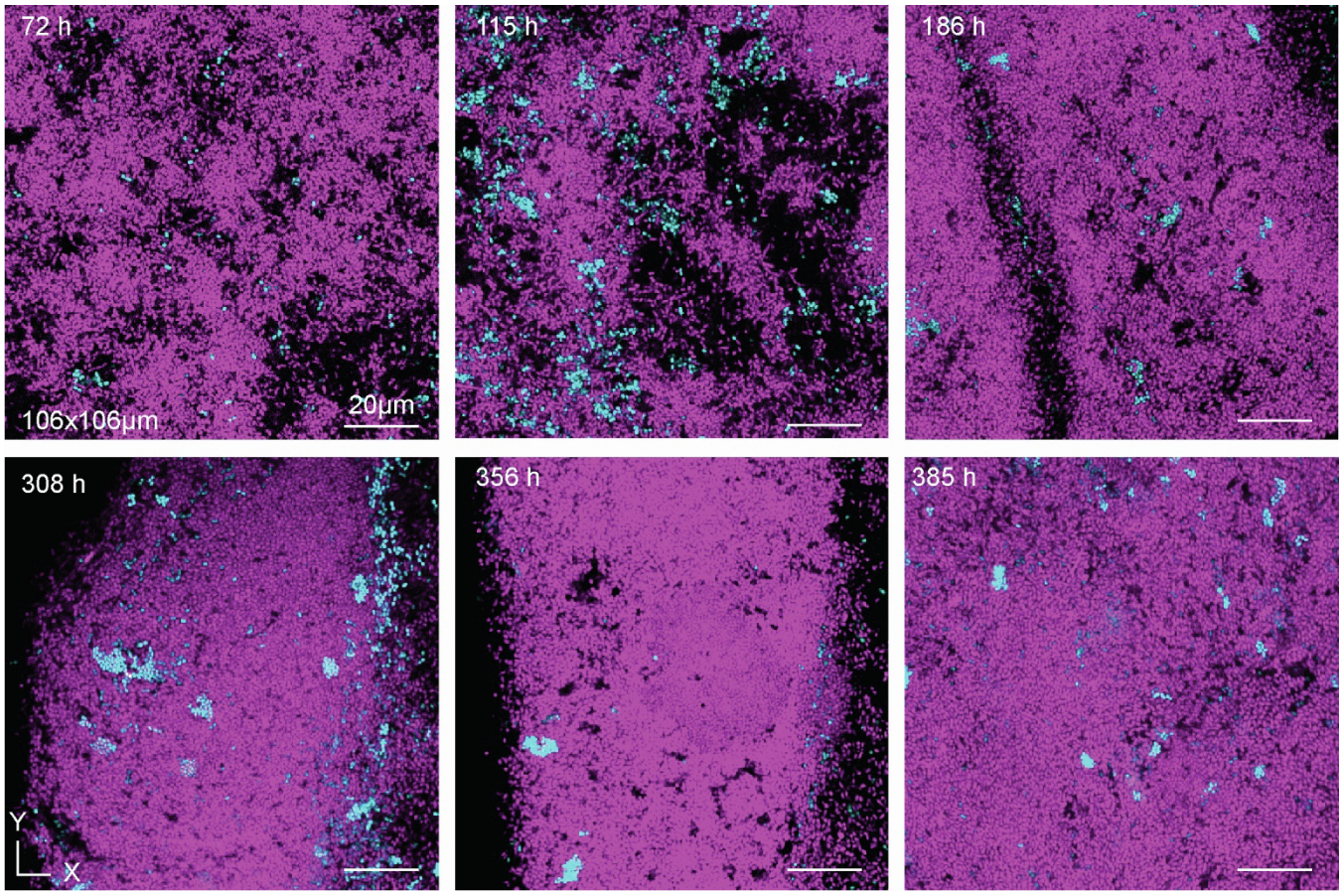

Figure S3. *E. coli-E. faecalis* biofilm architecture, related to Figure 1.
Representative images of the *E. coli-E. faecalis* biofilm time course. *E. coli* is shown in purple and *E. faecalis* is shown in cyan.

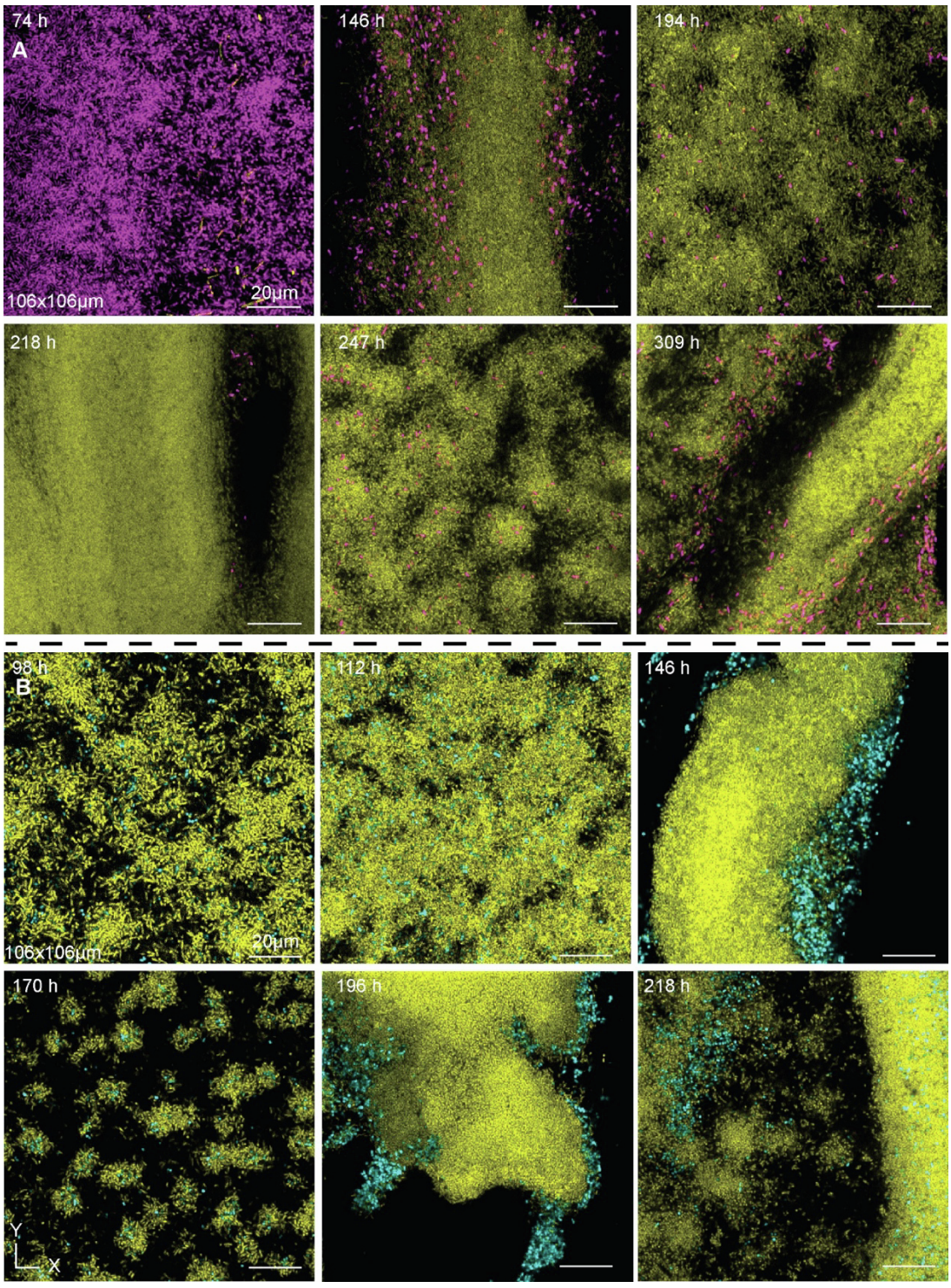

Figure S4. The *E. faecalis-P. aeruginosa* and *E. coli-P. Aeruginosa* biofilm culture conditions are not architecturally distinct from the triculture condition, related to Figure 1 and Figure 2.
(A) Representative images of the *E. coli-P aeruginosa* biofilm time course. *P. aeruginosa* is shown in yellow, and *E. faecalis* is shown in cyan. **(B)** Representative images of the *E. faecalis-P aeruginosa* biofilm time course. *P. aeruginosa* is shown in yellow, and *E. faecalis* is shown in cyan.

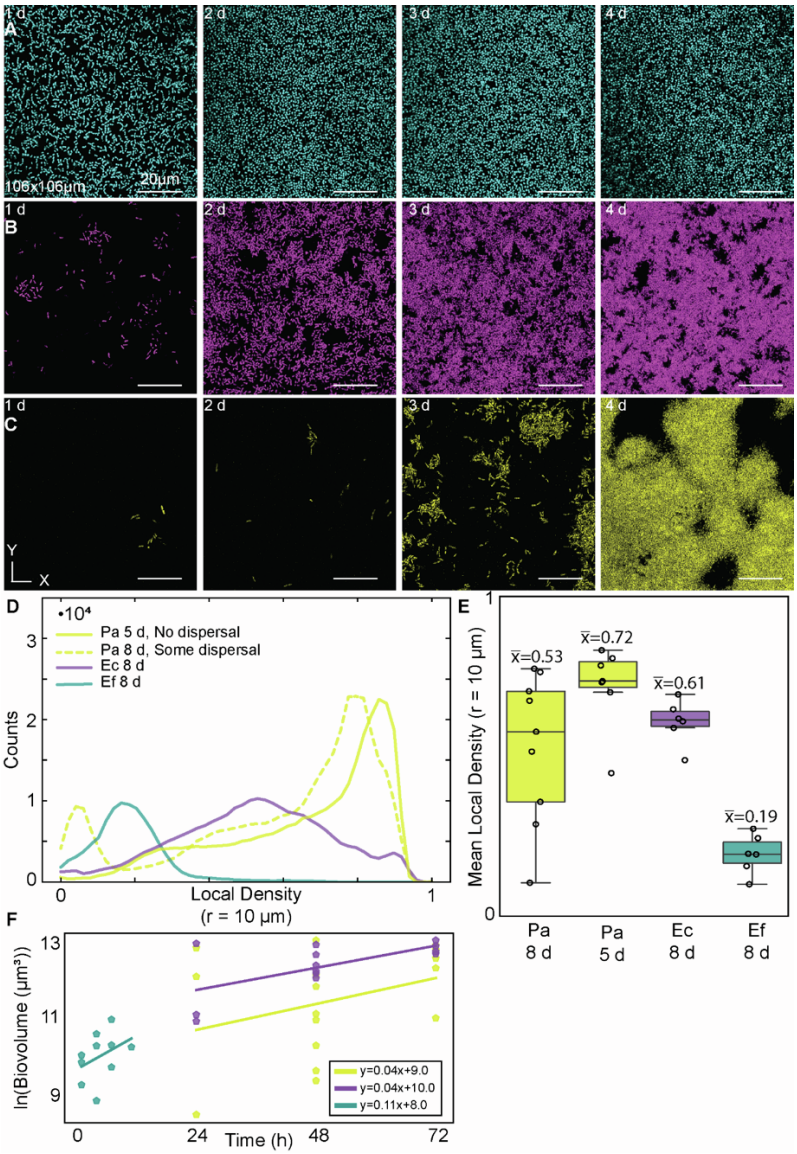

Figure S5. The three species achieve a range of growth rates and mean local density when grown in monoculture, related to Figure 1, Figure 2, Figure 3.

(A) Representative images of an *E. faecalis* monoculture biofilm (cyan). **(B)** Representative images of an *E. coli* monoculture biofilm (purple). **(C)** Representative images of a *P. aeruginosa* monoculture biofilm (yellow). **(D)** Histograms of mean local density (radius = 10 µm) for *E. coli* (purple), *P. aeruginosa* (yellow), and *E. faecalis* (cyan) (n=3-4). **(E)** Corresponding box and whisker plots of mean local density (radius = 10 µm) for *E. coli*, *P. aeruginosa*, and *E. faecalis* (n=3-4). **(F)** The maximal growth rate was determined by taking the slope of the natural log of the biovolume of monoculture biofilms during initial timepoints (n= 3-8).

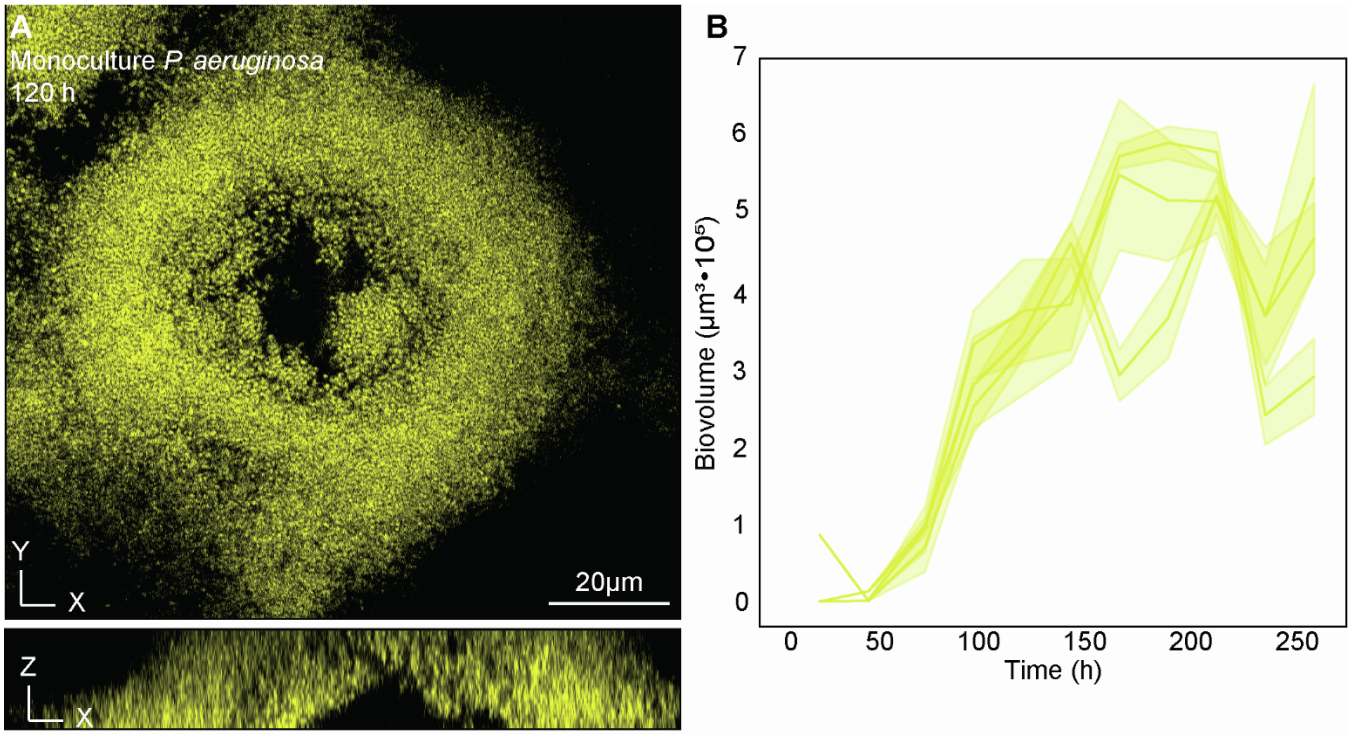

Figure S6. Monoculture *P. aeruginosa* (yellow) disperses from the microfluidic chamber, related to Figure 2.

(A) Representative image of a hollowed *P. aeruginosa* colony, characteristic of *P. aeruginosa* biofilm dispersal. **(B)** Traces of *P. aeruginosa* monoculture biofilms. Solid lines represent the mean and shaded regions represent one standard deviation above and below the mean (n = 3).

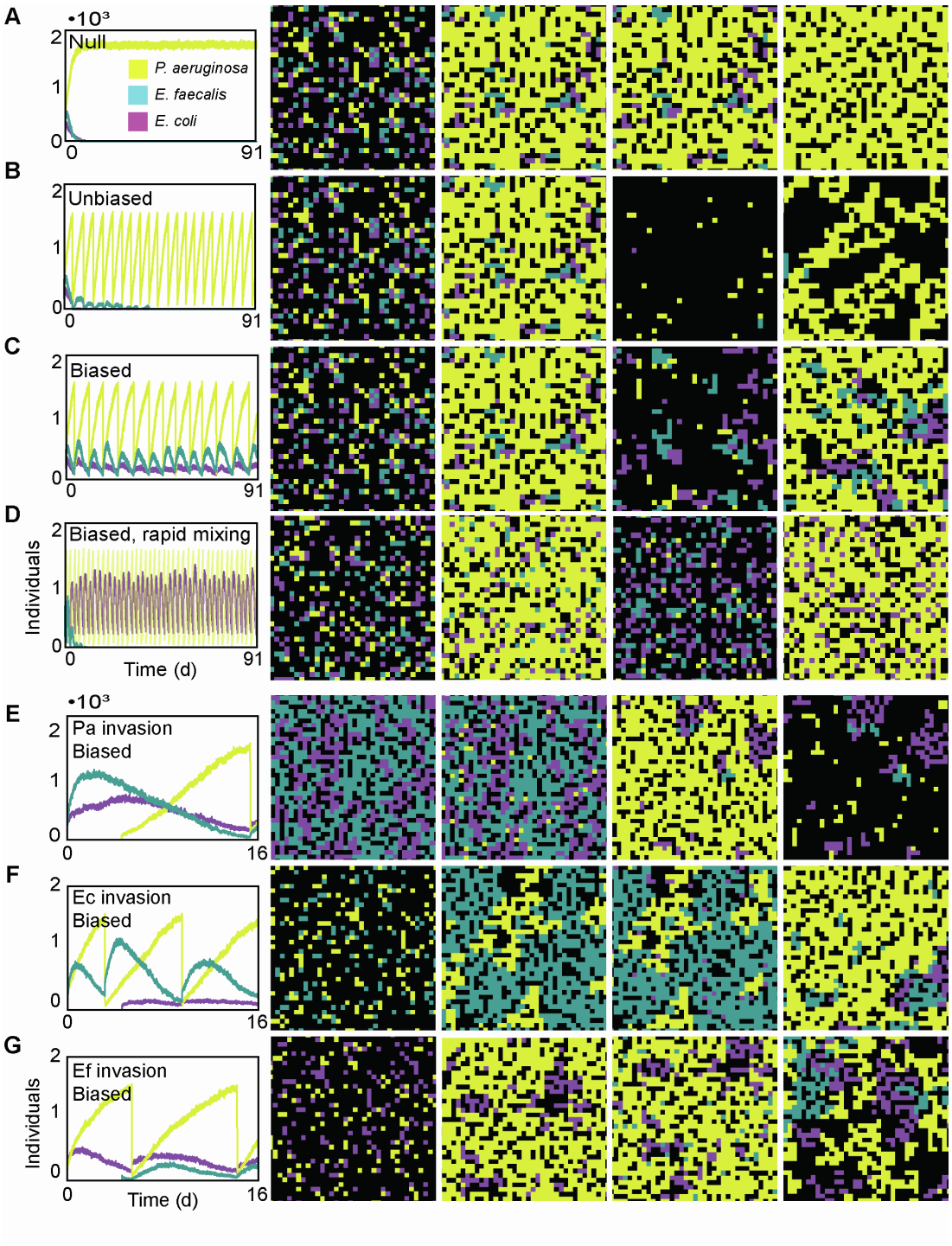

Figure S7: Coexistence in the stochastic-spatial model is dependent on dispersal bias and spatial arrangement, related to Figure 2 and Figure 3.

(A) No dispersal occurs. **(B)** All three species disperse equally. **(C)** Only *P. aeruginosa* disperses. **(D)** Random mixing of the grid in the biased dispersal case abolishes space and leads to a loss of *E. faecalis*. **(E)** *P. aeruginosa* invasion into an *E. coli* and *E. faecalis* community. **(F)** *E. faecalis* invasion into an *E. coli* and *P. aeruginosa* community. **(G)** *E. coli* invasion into an *E. coli* and *P. aeruginosa* community.

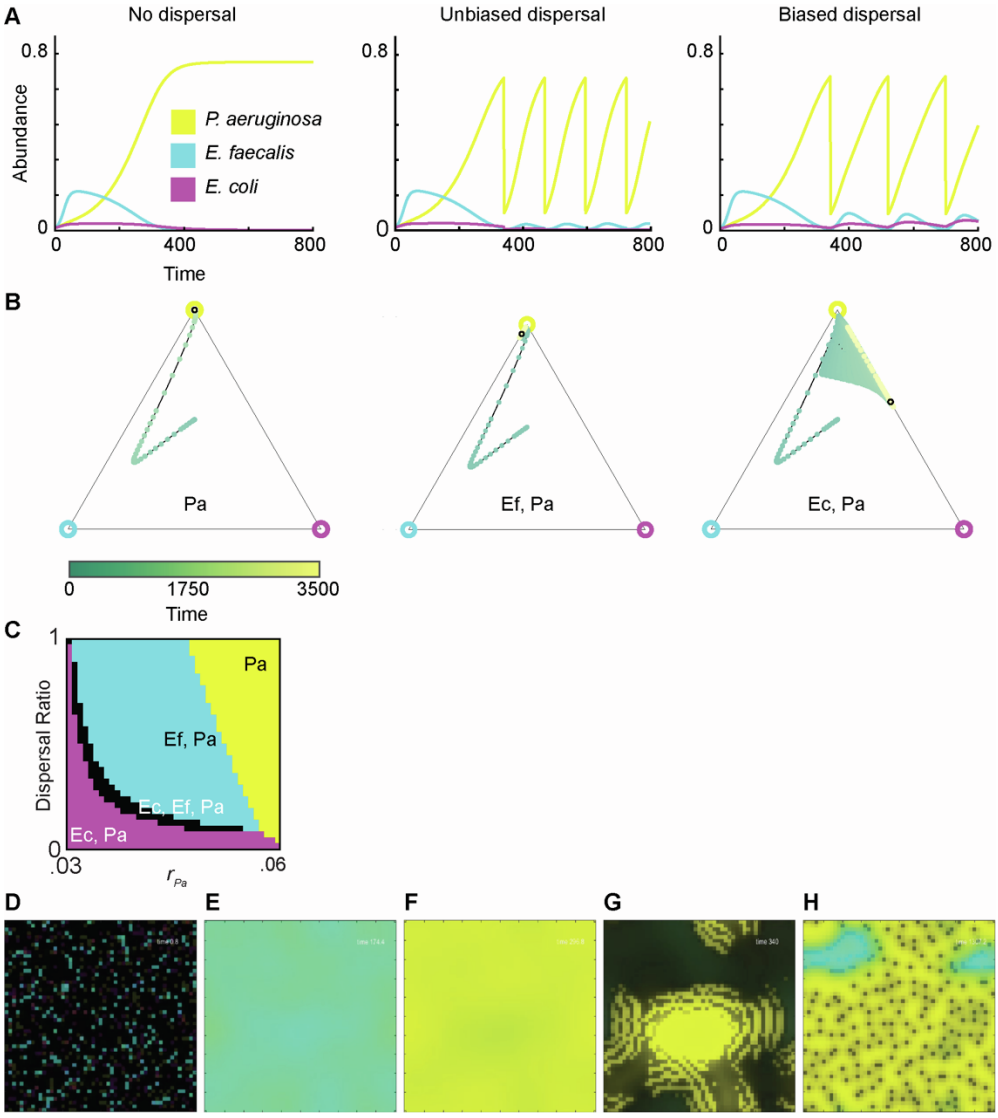

Figure S8. Deterministic models support dispersal as a mechanism of coexistence, related to Figure 2.

(A) Trajectories from a mean field model over experimentally relevant time scales. **(B)** Ternary plots of the mean field model, colored by time (green to yellow) with the black dot being the final timepoint, show two species coexistence over extended time scales in the unbiased and biased dispersal case. **(C)** Phase diagram of the biased dispersal model plotting *P. aeruginosa*'s carrying capacity, r_{Pa}, against dispersal ratio (δ_i/δ_{Pa}), ranging from the Biased Dispersal case (dispersal ratio of 0) to the Unbiased Dispersal case (dispersal ratio of 1) as the growth rate of *P. aeruginosa* (r_{Pa}) is varied from 0.03 to 0.06. The color map represents the presence or absence of species, with black representing the region of three-species coexistence. **(D-H)** Representative images from a reaction-diffusion implementation of our community dynamics model. Time is advancing in A through E, with major dispersal events becoming evident in panels D and E. *P. aeruginosa* is shown in yellow, *E. faecalis* is shown in cyan, and *E. coli* is shown in dark red. *E. coli* is difficult to discern after the first time step visually, but it remains present along with the other two species for the full duration of this and all other partial differential equation simulations with biased *P. aeruginosa* dispersal.

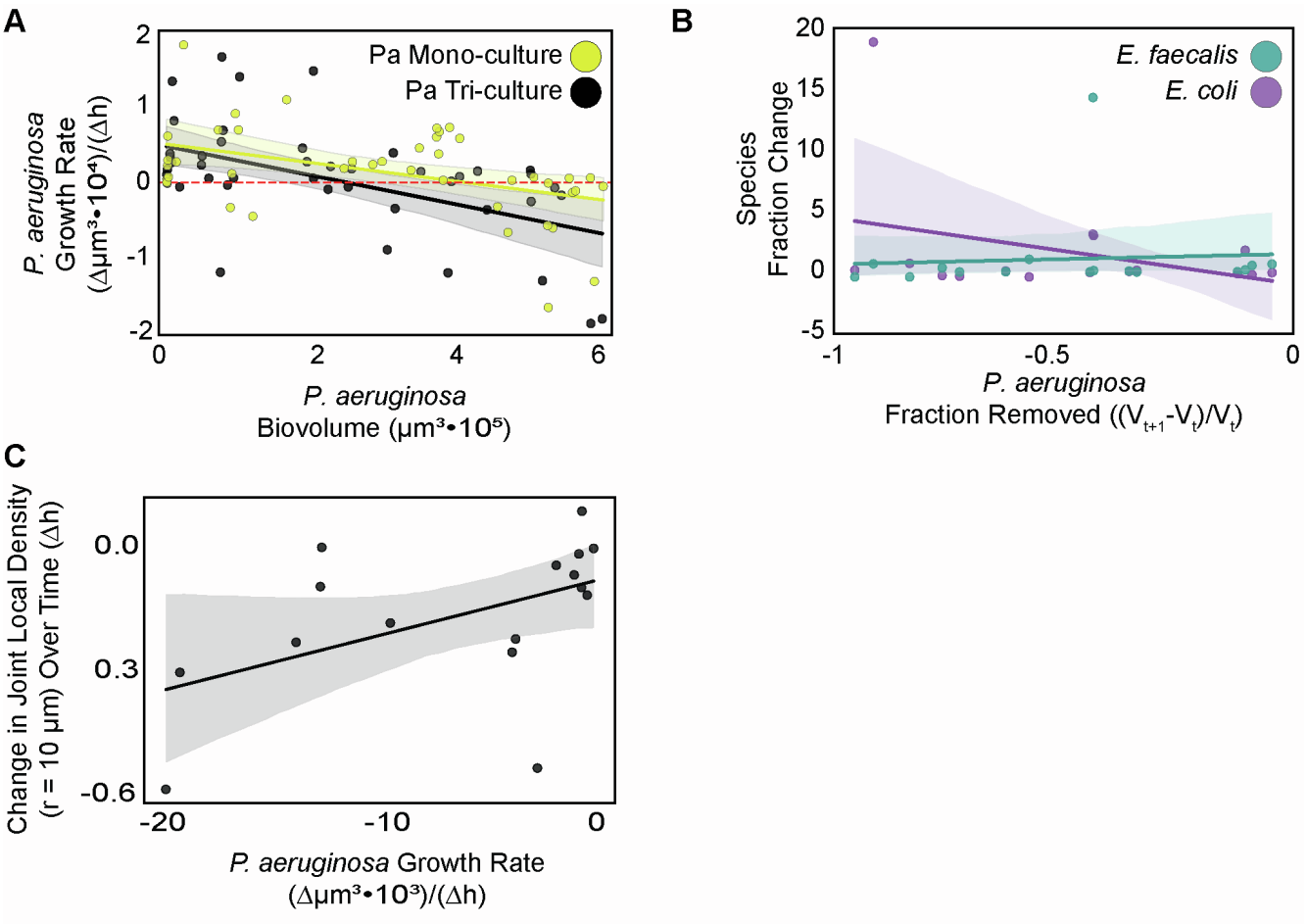

Figure S9. *P. aeruginosa* drives dispersal events, altering biofilm architecture, related to Figure 2.

(A) Monoculture *P. aeruginosa* disperses in a population density-dependent manner that is not significantly different than when in the three-species community. 95% confidence interval (shaded region) of linear regression fits overlap between monoculture and coculture dataset (mono-culture linear regression r^2=0.16, p=0.0032, tri-culture linear regression, r^2=0.25, p=0.0002, data from n = 3 independent experiments). **(B)** *P. aeruginosa* dispersal is biased in the sense that there is no correlation between the fraction of *P. aeruginosa* biovolume removed and the fraction of *E. coli* (r^2=0.09, p=0.1911, data from n = 3 independent experiments) or *E. faecalis* (r^2=0.01, p=0.7930, data from n = 3 independent experiments) biovolume removed. **(C)** *P. aeruginosa* dispersal events correlate moderately with changes in total biofilm density (r^2=0.25, p=0.0489, data from n = 3 independent experiments). Solid lines represent line fits and shaded regions represent a 95% confidence interval.

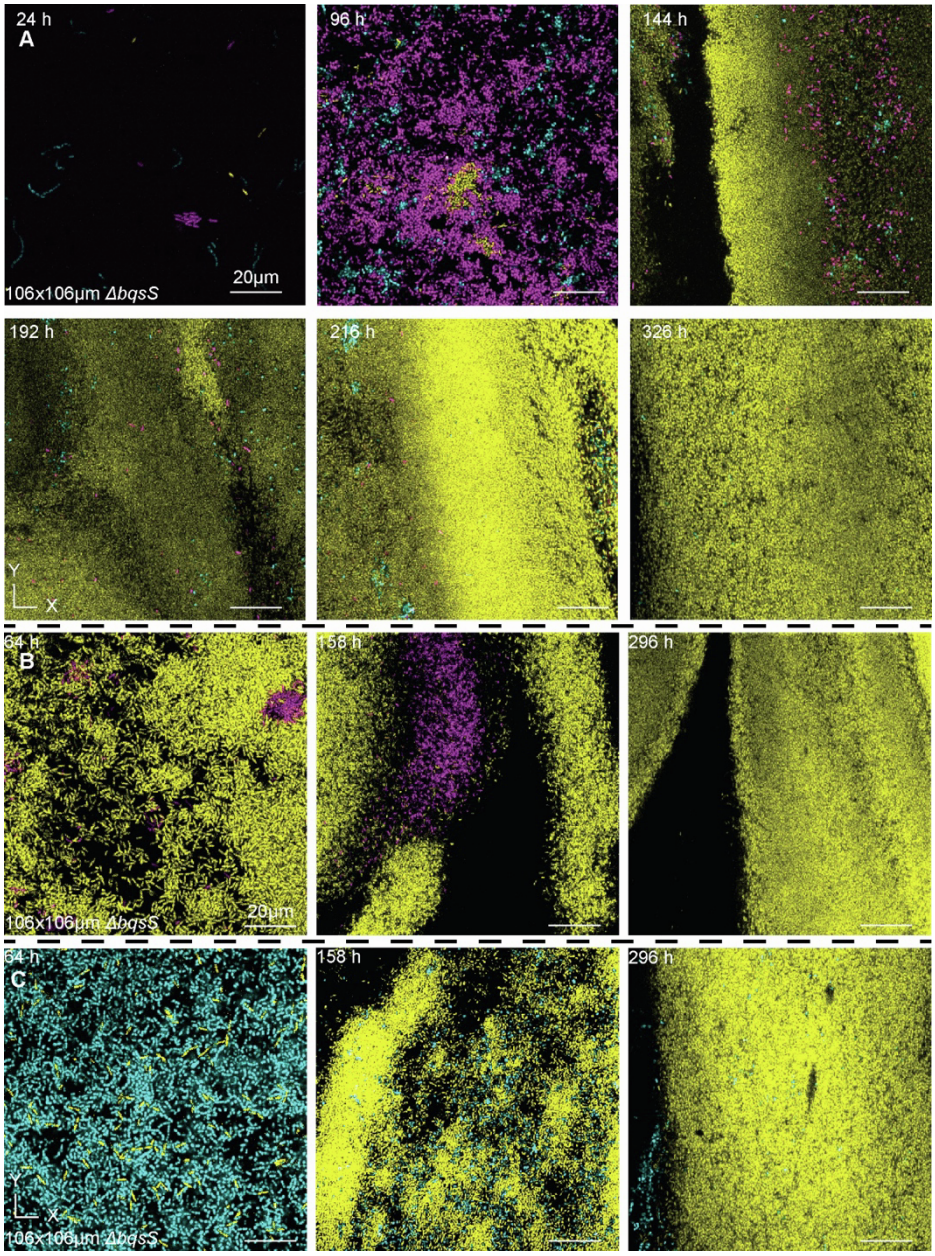

Figure S10. The *P. aeruginosa* Δ*bqsS* biofilm community does not undergo mass dispersal events, related to Figure 5.

(A) Representative images of the *P. aeruginosa* Δ*bqsS*-*E. coli* biofilm culture time course showing consistent biofilm architecture and decreased abundance of *E. coli* relative to *P. aeruginosa* WT biofilm cultures. **(B)** Representative images of the *P. aeruginosa* Δ*bqsS*-*E. faecalis* biofilm culture time course showing consistent biofilm architecture and decreased abundance of *E. faecalis* relative to *P. aeruginosa* WT biofilm cultures. **(C)** Representative images of the *P. aeruginosa* Δ*bqsS* biofilm community time course showing consistent biofilm architecture and decreased abundance of *E. coli* and *E. faecalis* relative to *P. aeruginosa* WT biofilm cultures. *P. aeruginosa* is shown in yellow and *E. coli* is shown in purple, and *E. faecalis* is shown in cyan

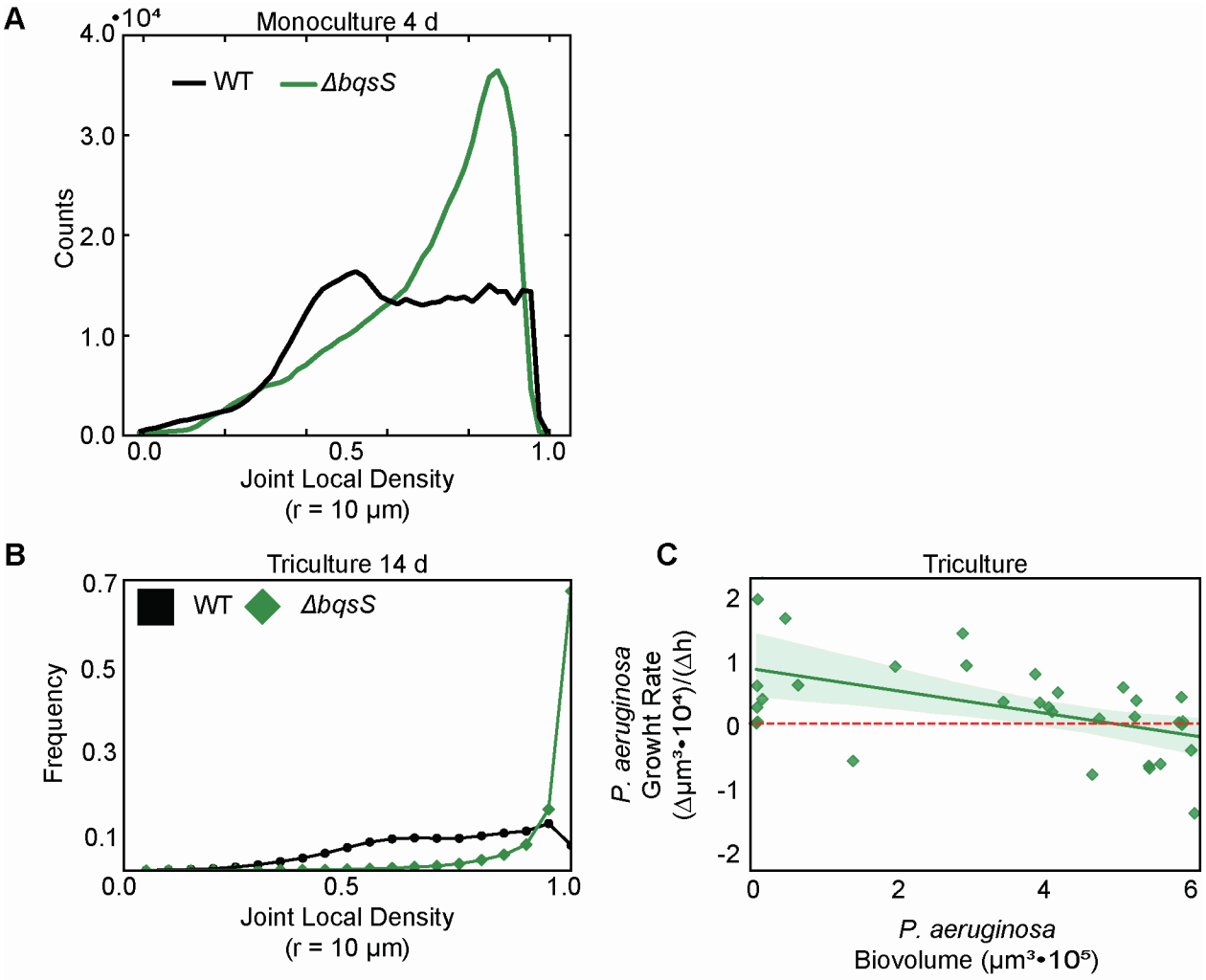

Figure S11. *P. aeruginosa* Δ*bqsS* has a shifted density profile and does not disperse in the same density-dependent manner as WT *P. aeruginosa*, related to Figure 5.

(A) Histograms of local population density (r = 10 μm) of Δ*bqsS* and WT *P. aeruginosa* monoculture biofilms (n = 3). **(B)** Histograms of joint local population density (r = 10 μm) of Δ*bqsS* and WT *P. aeruginosa* biofilm communities (n = 4). **(C)** *P. aeruginosa* Δ*bqsS* biovolume does correlate with its change in biovolume at the following timestep (r^2 = 0.25, p = 0.0013, n = 34 timesteps), but crosses 0 (dashed, red line) at a higher value (n = 3). The solid line represent the line fit and the shaded region represents a 95% confidence interval.

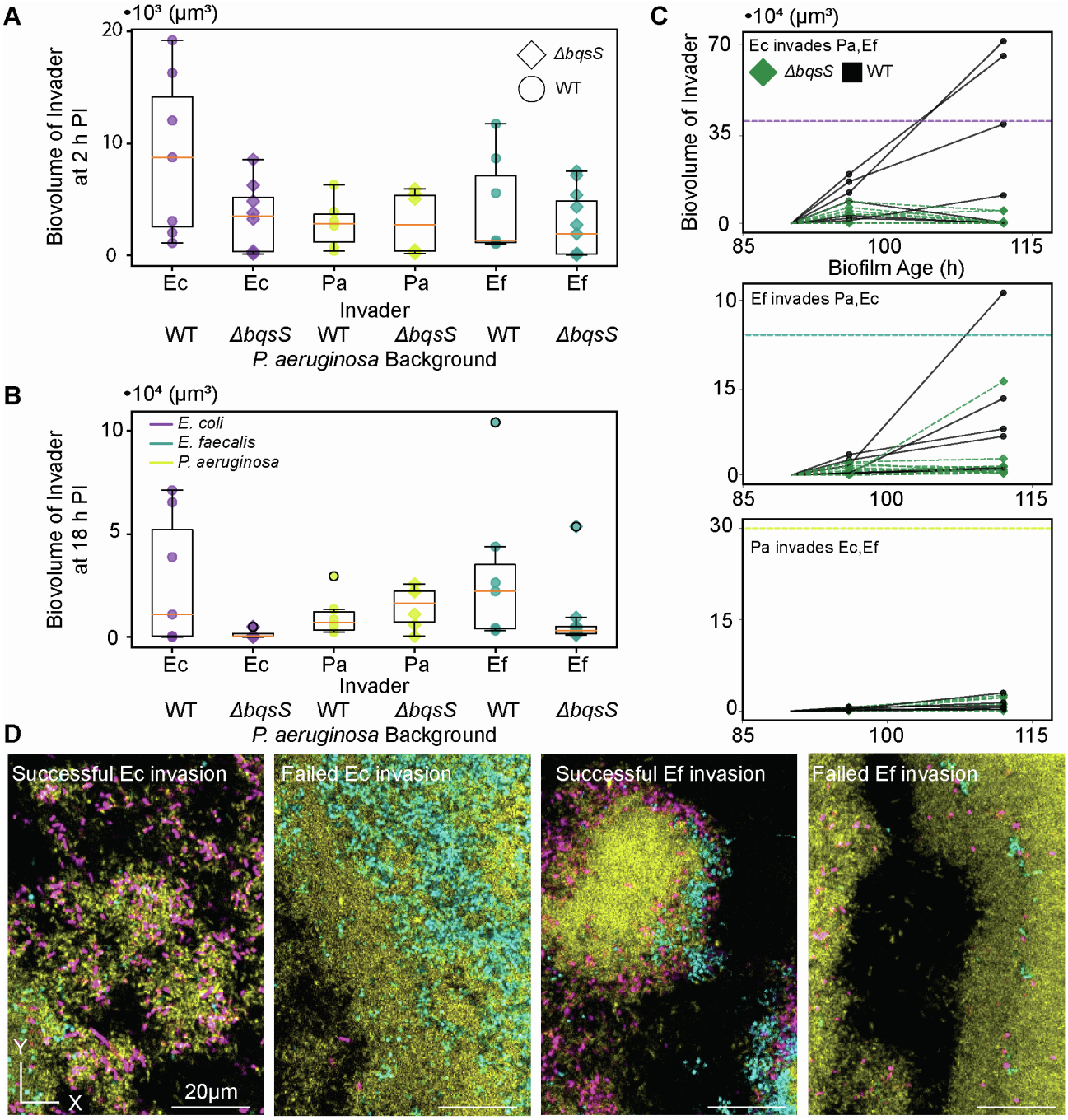

Figure S12. *P. aeruginosa* is conditionally susceptible to invasion by *E. coli* and *E. faecalis*, related to Figure 6.

(A) Box and whisker plots of the biovolume of the invading strain 2 h post invasion (n = 6-10). **(B)** Box and whisker plots of the biovolume of the invading strain 18 h post invasion (n = 6-10). **(C)** Trajectories of the invading strain biovolume with the average biovolume from the three-species biofilm competition experiments overlayed as a dashed line (n = 6-10). **(D)** Representative images of successful and failed invasions by *E. coli* and *E. faecalis* into biofilm cocultures containing WT *P. aeruginosa*.

Parameter	Symbol	Value
P. aeruginosa maximal growth rate	r_{Pa}	0.042
E. faecalis maximal growth rate	r_{Ef}	0.109
E. coli maximal growth rate	r_{Ec}	0.036
P. aeruginosa carrying capacity	K_{Pa}	0.72
E. faecalis carrying capacity	K_{Ef}	0.19
E. coli carrying capacity	K_{Ec}	0.61
Dispersal rate	δ_i	0.2
Dispersal trigger	N_{down}	$0.9*K_{pa}$
End of dispersal trigger	N_{up}	$0.1*K_{pa}$

Table S1. Model parameters, related to Figure 2.